

**THREE-PHOTON ELECTROMAGNETICALLY
INDUCED TRANSPARENCY IN RYDBERG
ATOMS**

**A Thesis Submitted to
the Graduate School of Engineering and Sciences of
İzmir Institute of Technology
in Partial Fulfillment of the Requirements for the Degree of**

MASTER OF SCIENCE

in Photonics Science and Engineering

**by
Yağız OYUN**

**July 2019
İZMİR**

We approve the thesis of Yağız OYUN


Examining Committee Members:



Assoc. Prof. Sevilay SEVINÇLİ
Department of Photonics, İzmir Institute of Technology



Assoc. Prof. Özgür ÇAKIR
Department of Physics, İzmir Institute of Technology



Assoc. Prof. Serkan ATEŞ
Department of Physics, İzmir Institute of Technology



Assoc. Prof. Sinan BALCI
Department Photonics, İzmir Institute of Technology




Assoc. Prof. Göktağ KARPAT
Department of Physics, İzmir University of Economics

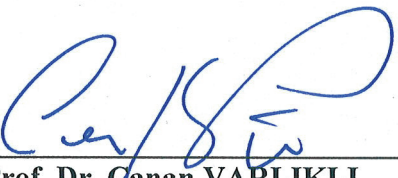
17 July 2019



Assoc. Prof. Sevilay SEVINÇLİ
Supervisor, Department of Photonics,
İzmir Institute of Technology



Assoc. Prof. Özgür ÇAKIR
Co-Supervisor, Department of Physics
İzmir Institute of Technology



Prof. Dr. Canan VARLIKLI
Head of the Department of Photonics

Prof. Dr. Aysun SOFUOĞLU
Dean of Graduate School of
Engineering and Science

ACKNOWLEDGMENTS

First of all, I would like to express my gratitude to my advisor Assoc. Prof. Sevilay Sevinçli for her extreme patience and mentorship. Her advices on life itself gave me the push I needed, during the period for this thesis.

I can never forget the joy I have felt during the first half of my graduate studies with Assoc. Prof. Serkan Ateş. I am deeply grateful for, working in the lab together, having tremendously interesting discussions and for his counseling on important stuff.

I acknowledge, Assoc. Prof. Özgür Çakır for his invaluable contributions and compelling discussions in the subject of this thesis.

I would also like to thank my brother and best friend Hoto, since he was always there for me. I am grateful for your never-ending encouragement, it has always been a comfort, to know you exist.

Şebnem, I am extremely thankful for your love, joy and unquestioned support. It would have been very difficult without you. I am glad that you are with me.

Lastly, I express my deepest thanks to my family for their unending assistance, unconditional love and unwavering patience.

This research was supported by TUBITAK with 117F372 project number.

ABSTRACT

THREE-PHOTON ELECTROMAGNETICALLY INDUCED TRANSPARENCY IN RYDBERG ATOMS

Electromagnetically Induced Transparency (EIT) is a quantum coherence phenomenon, in which an atomic medium is rendered transparent via destructive interference of excitation pathways. EIT was first observed in a three-level lambda scheme where a modified optical response is achieved by the interference of light field induced atomic state coherences at the resonance of transition. An EIT system also produces important optical effects including giant Kerr non-linearity and slow light. Rydberg-EIT media have been used to study optical properties of atomic media, non-linear optical effects and to gain better understanding on interacting many-body systems due to the controllable interactions of Rydberg atoms. Recently EIT in a four-level ladder scheme was realized experimentally in a dressed-state manner with Cs atomic vapor, in which a strong dressing field allows for a transparency window to be opened for probe field. Rydberg EIT has potential applications in terahertz regime, electrometry, metrology and quantum information science, but extensive studies on four-level Rydberg EIT schemes are scarce. In this thesis; three-photon EIT in a cold atomic ensemble that has a ladder type excitation scheme, in which the highest energy state is a Rydberg state is investigated. Atom-light interactions of a four-level ladder system is developed for non-interacting case, then extended to many-body case. Starting with the steady-state solutions without atomic interactions, Rydberg EIT system is analyzed using mean-field and rate equation methods, though due to inadequate computing power and lack of time we could not finalize the rate equation method. To understand effects of Rydberg-Rydberg interactions on these systems in detail, two-body case is investigated with mean-field method. Afterwards, to achieve more realistic results, a self-consistent mean-field method for larger systems is developed. It is observed that as the van der Waals interaction energy increases, Rydberg blockade becomes more prominent. Therefore induced transparency weakens, broadens and shifts away from the resonance as expected. This means that, controllable interactions in a Rydberg EIT medium enables to control and modify the optical response of the atomic medium.

ÖZET

RYDBERG ATOMLARINDA ÜÇ-FOTON UYARIMLI ELEKTROMANYETİK OLARAK İNDÜKLENMİŞ ŞEFFAFLIK

Elektromanyetik olarak indüklenmiş şeffaflık (EIT), opak bir atomik ortamın, uyarım yollarının yıkıcı girişime uğraması ile şeffaflaştığı bir kuantum eşuyumluluk olayıdır. EIT ilk kez, üç seviyeli lambda sisteminde gözlenmiştir. Atomik ortamın optik tepkisinin değişime uğradığı bu sistemde şeffaflık, ışık alanının etkisiyle indüklenmiş atomik eşuyumluluklarının geçiş rezonansında yıkıcı girişimi ile elde edilmiştir. EIT sistemleri ile, doğrusal olmayan büyük Kerr etkileri ve yavaş ışık gibi önemli etkiler gözlenmiştir. Rydberg EIT ortamı, atomik sistemlerin optik özelliklerini, doğrusal olmayan optik etkileri çalışmak için ve Rydberg atomlarının kontrol edilebilir etkileşimleri sayesinde etkileşimli çok atom sistemlerini daha iyi anlamak için kullanılmıştır. Yakın geçmişte, Rydberg EIT, Cs atomik buharında, dört seviyeli basamak sistemi ile deneysel olarak gösterilmiştir. Bu sistemde güçlü giydirme alanı, prob alanı için şeffaflık penceresi açılmasını sağlamıştır. Rydberg EIT terahertz rejiminde, elektrometride, metrolojide ve kuantum bilgi bilimlerinde potansiyel uygulamalar vaat etmektedir ancak dört düzeyli Rydberg EIT sistemlerinde geniş kapsamlı çalışmalar nadirdir. Bu tezde; soğuk atomlarda üç-foton uyarımlı basamak Rydberg EIT sistemi incelenmiştir. Atom-ışık etkileşimleri, etkileşimsiz dört seviyeli basamak sistemleri için geliştirilmiştir ve sonra etkileşimli çok atomlu sistemler için genişletilmiştir. Başlangıçta, atomik etkileşimler olmayan sistemler için durağan durum çözümleri elde edilmiştir. Daha sonra Rydberg atom etkileşimleri olan sistemler için ortalama alan ve oran denklemleri yöntemleri kullanılarak Rydberg EIT ortamı çalışılmıştır. Ancak işlem gücü ve zaman yetersizliğinden dolayı oran denklemleri yöntemi sonuca ulaştırılamamıştır. Rydberg EIT sistemlerinde, Rydberg-Rydberg etkileşimlerini incelemek için, öncelikle basit bir durum olan etkileşimli iki atom durumu ortalama alan yöntemi kullanılmıştır. Daha sonra, büyük sistemler için daha gerçekçi sonuçlar elde etme hedefiyle, kendi içinde tutarlı ortalama alan yöntemi geliştirilmiştir. van der Waals etkileşimlerinin kuvveti arttıkça, Rydberg blokaj mekanizması etkisini arttırmış ve elektromanyetik olarak indüklenmiş şeffaflık rezonanstan kayarak etkisini yitirmiştir. Bu, Rydberg EIT ortamlarındaki kontrol edilebilir Rydberg etkileşimlerinin, ortamın optik tepkisinin kontrollü bir şekilde değiştirilebilmesini sağladığı görülmüştür.

To my family...

TABLE OF CONTENTS

LIST OF FIGURES	viii
LIST OF TABLES	xii
CHAPTER 1. INTRODUCTION	1
1.1. Electromagnetically Induced Transparency	4
1.2. Optical Response	6
1.3. Rydberg Atoms	8
CHAPTER 2. THEORY	12
2.1. Three-Photon Electromagnetically Induced Transparency	12
2.1.1. Electromagnetically Induced Transparency with Interacting Rydberg Atoms	19
CHAPTER 3. MEAN-FIELD APPROACH	24
3.1. Mean-Field Approximation	24
3.1.1. Two-Body System	25
3.1.2. Self-Consistent Mean-Field Algorithm	32
CHAPTER 4. RATE EQUATION MODEL	42
CHAPTER 5. CONCLUSION	45
REFERENCES	47
APPENDIX A. MATLAB SCRIPTS	55
A.1. Steady State Solutions for OBEs	55
A.2. Self-Consistent Mean-Field Algorithm	57
A.3. Monte-Carlo Algorithm	64

LIST OF FIGURES

<u>Figure</u>	<u>Page</u>
<p>Figure 1.1. (Left) Three-level lambda scheme. (Right - top) Absorption of the medium for the probe field with respect to different probe field detunings. (Right - bottom) Refractive Index of the medium for the probe field with respect to different probe field detunings. Addition of another transition, allows the medium to become transparent for the probe field on resonance.</p>	6
<p>Figure 2.1. Three-photon excitation or four-level ladder scheme. Excitations, $1\rangle \rightarrow 2\rangle$, $2\rangle \rightarrow 3\rangle$, $3\rangle \rightarrow 4\rangle$ are accomplished with three different light fields with Rabi frequencies; Ω_1, Ω_2 and Ω_3, respectively. Excited states $4\rangle$, $3\rangle$ and $2\rangle$ have spontaneous decay rates of Γ_3, Γ_2 and Γ_1, respectively.</p>	13
<p>Figure 2.2. (Top) Imaginary part and (Bottom) real part of probe coherence, with respect to detuning of the probe field for a four-level ladder system in steady state. The dip occurring at the three-photon resonance frequency $\Delta_1 = 2\pi \times 4$ represents the vanishing of absorption in the medium. At the frequency where EIT is observed, steep dispersion curve or rapid change in refractive index is observed (Šibalić et al., 2016). Other parameters are provided in text.</p>	20
<p>Figure 2.3. (Top) Eigenvalues for the system Hamiltonian of four-level scheme with respect to probe field detuning. (Middle) Imaginary part of probe coherence with respect to probe field detuning. (Bottom) Zoomed in avoided eigenvalue crossings. Grey vertical lines indicate avoided crossing frequencies. Avoided crossings correspond exactly to the absorption maxima. A dark-state or zero eigenvalue corresponds to the EIT window that occurs around three-photon resonance $\Delta_1 = 2\pi \times 4$ MHz. Parameters are the same as in Figure 2.2</p>	21

Figure 3.1. Evolution of ground state, Rydberg state populations and imaginary and real parts of probe coherence ρ_{12} with respect to time. Time evolution for three-photon resonance $\Delta_1 = 2\pi \times 4$ MHz is shown because EIT window is observed at three-photon resonance. Other parameters are provided in text.	26
Figure 3.2. Imaginary part of probe coherence with $r = 5 \mu m$ at different n , with respect to probe field detuning. Inset shows the region around three-photon resonance ($\Delta_1 = 2\pi \times 4$ MHz). Other parameters are provided in text.	28
Figure 3.3. Imaginary part of probe coherence at $n = 60$, with different r , with respect to probe field detuning. Inset shows the region around three-photon resonance ($\Delta_1 = 2\pi \times 4$ MHz). Other parameters are provided in text.	29
Figure 3.4. Real part of probe coherence with $r = 5 \mu m$ at different n , with respect to probe field detuning. Inset shows the region around three-photon resonance ($\Delta_1 = 2\pi \times 4$ MHz). Other parameters are provided in text.	30
Figure 3.5. Real part of probe coherence at $n = 60$, with different r , with respect to probe field detuning. Inset shows the region around three-photon resonance ($\Delta_1 = 2\pi \times 4$ MHz). Other parameters are provided in text. .	31
Figure 3.6. Imaginary part and real part of probe coherence with respect to probe field detuning for $r = 1 \mu m$ in the four-level case and a three-level case. (Left) , shows imaginary part of probe coherence and (Right) shows real part of probe coherence with different probe detunings. Other parameters are provided in text.	31
Figure 3.7. Ground state populations, with respect to probe field detuning for two cases: (Left) for different inter-atomic distances $r = 1, 2, 4, 6 \mu m$ with $n = 60$, (Right) for different principal quantum numbers $n = 50, 60, 70, 80$ including non-interacting scenario with inter-atomic distance $r = 5 \mu m$. Insets show the region around three-photon resonance ($\Delta_1 = 2\pi \times 4$ MHz). Other parameters are provided in text.	32

Figure 3.8. Rydberg state populations, with respect to probe field detuning for two cases: (Left) for different inter-atomic distances $r = 1, 2, 4, 6 \mu m$ with $n = 60$, (Right) for different principal quantum numbers $n = 50, 60, 70, 80$ including non-interacting scenario with inter-atomic distance $r = 5 \mu m$. Insets show the region around three-photon resonance ($\Delta_1 = 2\pi \times 4$ MHz). Other parameters are provided in text.	33
Figure 3.9. Self-consistent mean-field algorithm flowchart.	34
Figure 3.10. Imaginary part of probe coherence with respect to probe field detuning, with non-interacting case and $n = 50, 60, 70, 80, 90, 100$. Inset shows the zoomed in region around three-photon resonance $\Delta_1 = 2\pi \times 4$ MHz. Other parameters are provided in text.	35
Figure 3.11. Real part of probe coherence with respect to probe field detuning, with non-interacting case and $n = 50, 60, 70, 80, 90, 100$. Inset shows the zoomed in region around three-photon resonance $\Delta_1 = 2\pi \times 4$ MHz. Other parameters are provided in text.	36
Figure 3.12. Ground state population with respect to probe field detuning, with non-interacting case and $n = 50, 60, 70, 80, 90, 100$. Inset shows the zoomed in region of three-photon resonance $\Delta_1 = 2\pi \times 4$ MHz. Other parameters are provided in text.	37
Figure 3.13. Rydberg state population with respect to probe field detuning, with non-interacting case and $n = 50, 60, 70, 80, 90, 100$. Inset shows the zoomed in region of three-photon resonance $\Delta_1 = 2\pi \times 4$ MHz. Other parameters are provided in text.	38
Figure 3.14. Imaginary part of probe coherence with respect to probe field detuning, with different dressing detunings $\Delta_2 = 2\pi \times (-2, 0, 2, 4)$. Other parameters are provided in text.	39
Figure 3.15. Real part of probe coherence with respect to probe field detuning, with different dressing detunings $\Delta_2 = 2\pi \times (-2, 0, 2, 4)$. Other parameters are provided in text.	40
Figure 3.16. Ground state population with respect to probe field detuning, with different dressing detunings $\Delta_2 = 2\pi \times (-2, 0, 2, 4)$. Other parameters are provided in text.	40

Figure 3.17. Rydberg state population with respect to probe field detuning, with different dressing detunings $\Delta_2 = 2\pi \times (-2, 0, 2, 4)$. Other parameters are provided in text.	41
Figure 4.1. Rate equation model Monte-Carlo algorithm flowchart.	44

LIST OF TABLES

<u>Table</u>		<u>Page</u>
Table 1.1.	Scaling laws of Rydberg state properties with principal quantum number.	9
Table 1.2.	van der Waals interaction energies and blockade radii for an ensemble of Cs atoms with an average inter-atomic distance of $5 \mu m$ and with a Rydberg transition field Rabi frequency of $\Omega = 2\pi \times 0.5$ MHz on resonance. It is clearly seen that the interaction is very strong and even climbing up to 15 GHz at $n = 100$ with a blockade radius of $r_b = 20.7036 \mu m$	11
Table 3.1.	van der Waals interaction energies and blockade radii for two interacting Cs atoms for different n . Other parameters are provided in text.	27

CHAPTER 1

INTRODUCTION

Electromagnetically Induced Transparency (EIT) is a quantum coherence phenomenon, in which an opaque medium becomes transparent via interference of different excitation pathways. The simplest case of atom-light interaction is that of a two level atom and a driving field, when the driving field is on resonance with the transition, absorption maximum is observed, accompanied by Rabi oscillations, in which the atomic population oscillates between ground state and excited state (Gerry and Knight, 2004). But when a strong coupling field is introduced to the system, EIT is observed. Two-level atom absorption maximum and EIT in a three-level lambda system, on resonance can be seen in Figure 1.1. When the coupling field is stronger than the probe field, probability amplitudes of the transitions interfere destructively with one another, inducing transparency for the probe light (Harris et al., 1990). This can be understood via dressed-state picture and formation of a dark-state. EIT was first predicted in 1990 (Harris et al., 1990) and one year later demonstrated as a proof of concept in a three-level lambda scheme with Sr vapor (Boller et al., 1991).

As the absorptive features of the medium is altered by EIT, refractive features of the medium are modified as well (Fleischhauer et al., 1992). While the medium becomes transparent for the probe light, refractive index for the probe light undergoes a steep dispersion, which in turn slows the group velocity of light and this effect is demonstrated extensively (Budker et al., 1999; Kash et al., 1999; Hau et al., 1999). Light speed of 17 m s^{-1} was observed on an ultra-cold Na gas (Hau et al., 1999) and even light speed down to 8 m s^{-1} was observed on Rb vapor (Budker et al., 1999). Further studies on group velocity reduction by EIT mechanism, revealed that light pulses can be halted for a few milliseconds, by momentary turning off of the coupling light, transferring the information on the halted pulse to the atomic medium and when the coupling light is back on, light pulse is restored with the previous information (Phillips et al., 2001; Liu et al., 2001). Another important realization of the slow light phenomenon is the promising application of quantum memories for light. This was first proposed in 2000 with the realization of

reversible group velocity reduction in dark-state polaritons. A dark-state polariton is light field and atomic excitation couple. Reversible reduction in group velocity of dark-state polaritons in EIT configuration can be utilized to store and transfer information (Fleischhauer and Lukin, 2000; Lukin, 2003; Simon et al., 2010). Furthermore, building on the utility that comes with EIT for realization of quantum memories, EIT is also used for generation and storage of single photons with the intention of quantum communication between quantum memories (Eisaman et al., 2005; Chanelière et al., 2005).

Kerr effect is the change of refractive index by application of an electric field (LL.D., 1875). Kerr non-linearity is the similar type of modification in the dispersive features in third order susceptibility (Boyd, 2008). EIT scheme also allows a resonantly enhanced Kerr non-linearity (Harris et al., 1990; Hakuta et al., 1991), which has potential for applications in quantum information science via quantum gates (Schmidt and Imamoglu, 1996). In four-level Rubidium atoms, large Kerr non-linearity with diminishing linear susceptibility was shown using an EIT scheme (Kang and Zhu, 2003). Strong optical nonlinearity was also shown in a three-level Rydberg EIT scheme (Firstenberg et al., 2016).

Experimental demonstration of EIT with Rydberg atoms for coherent optical detection have been shown in 2007 (Mohapatra et al., 2007). Atoms which have high principal quantum number ($n > 10$) are called Rydberg atoms. Detailed information on Rydberg atom properties and applications is given in Section 1.3. Before experimental realization, Rydberg EIT was first proposed in order to realize a photonic phase gate, making use of the long-range interactions between Rydberg atoms and slow light features of EIT media (Friedler et al., 2005). Rydberg EIT also enabled spectroscopy of Rydberg states (Mauger et al., 2007). Rydberg EIT scheme can also be used for locking the laser frequency to a transition, by probing the EIT signal (P. Abel et al., 2009). Rydberg state depopulation due to Rydberg-Rydberg interactions was demonstrated using Rydberg EIT scheme (Weatherill et al., 2008). Atom-light interactions have shown to be controllable via electric fields using dark state polaritons in a Rydberg EIT scheme (Bason et al., 2008). Enhanced electro-optic effect, which is the modification of index of refraction via electric fields, was realized using a ladder Rydberg EIT scheme (Mohapatra et al., 2008). More recently, Rydberg EIT in a four-level ladder scheme was demonstrated with Cs atomic vapor cell (Carr et al., 2012). Moreover dressed-state EIT for a four-level ladder scheme

with Rydberg atoms shown to be promising for light storage (Šibalić et al., 2016).

Rydberg EIT scheme has promising applications in metrology, quantum computation (Firstenberg et al., 2016), electrometry (Mohapatra et al., 2008; Sedlacek et al., 2012) and in terahertz applications such as terahertz frequency signal storage (Bhushan et al., 2018) and terahertz detector (Wade et al., 2018). Four-level Rydberg EIT systems might have potential applications in THz sensing and imaging, Rydberg spectroscopy, nonlinear optical effects and optical response of atomic media due to the nature of Rydberg atoms combined with EIT. Three-photon excitation scheme also allows for cheaper experimental setups, because of the availability of inexpensive high-power infrared diode lasers. Although subject of Rydberg EIT is studied for more than a decade, comprehensive work on four-level Rydberg EIT systems are rare. Therefore in this thesis, cold atomic Rydberg EIT in a four-level ladder scheme is studied. Rydberg atom interactions and Rydberg blockade effects on EIT behavior is analyzed. In Section 1.1, basic concepts of EIT are provided for a three-level lambda scheme, including Hamiltonian for a lambda system and discussion of resulting dark state. Following that in Section 1.2, optical properties of the atomic medium are discussed. Connection of linear susceptibility to absorption and refractive index through atomic coherence is provided. Next, in Section 1.3, basics and general properties of Rydberg atoms are presented with van der Waals interactions and the Rydberg blockade effect. In Chapter 2, treatment and evolution of open quantum systems are introduced, followed by the atom-light interactions in a four-level ladder system. After the derivation of equations of motion for a non-interacting system of atoms, case for interacting Rydberg atoms is considered. In Chapter 3, mean-field approach for an interacting system is presented, starting with simplest case of two-body interactions. Interaction effects and blockade effects on optical properties of the medium are discussed as well as on ground state and Rydberg state populations. Following on the two-body case, mean-field approximation is extended for larger systems by employing a self-consistent method. Just as in the two-body case, interaction and blockade effects are analyzed on ground state, Rydberg state populations and on optical properties of the system. Following the mean-field approach, in Chapter 4, rate equation method is presented for interacting systems, where the rates of change of populations are used to extract the optical properties and understand the behavior of the system. Unfortunately, results for rate equation method could not be obtained due to inadequacy of time and computing power. Finally in Chapter 5,

summary of this thesis and a brief conclusion are provided.

1.1. Electromagnetically Induced Transparency

In order to better understand EIT mechanism, dressed state picture must be introduced. Here we will analyze briefly the dark state formation in a three-level lambda system. Hamiltonian of an atom interacting with light can be written as:

$$\hat{H} = \hat{H}_0 + \hat{H}_{AL} . \quad (1.1)$$

Here \hat{H}_0 is the atomic Hamiltonian which contains state energies and atom-light Hamiltonian $\hat{H}_{AL} = \vec{d} \cdot \vec{E}$, involving atom-light interaction energies. Within dipole approximation, which facilitate the atom-light interaction and within rotating wave approximation (RWA), which eliminate rapidly oscillating terms (Allen and H Eberly, 1987), the Hamiltonian of an atom in a three-level Lambda scheme as in Figure 1.1 is given as:

$$\hat{H} = -\hbar \begin{pmatrix} 0 & 0 & \frac{\Omega_1}{2} \\ 0 & -(\Delta_1 - \Delta_2) & \frac{\Omega_2}{2} \\ \frac{\Omega_1}{2} & \frac{\Omega_2}{2} & -\Delta_1 \end{pmatrix} . \quad (1.2)$$

In this system; transition to excited state $|3\rangle$ from ground state $|1\rangle$ is performed with probe light with Rabi frequency Ω_1 , transition to excited state from ground state $|2\rangle$ is performed by coupling light with Rabi frequency Ω_2 . Δ_1 and Δ_2 are detunings, which represent the difference between the transition frequency and field's frequency. Spontaneous decay rates of the state $|3\rangle$ are represented with Γ_1 and Γ_2 to ground states $|1\rangle$ and $|2\rangle$, respectively. Strong coupling light creates two dressed states and the destructive interference of the probability amplitudes of those transitions causes a modified opacity for the probe light. Following calculations will be performed under the assumption of both light sources being resonantly coupled to the excited state ($\Delta_1 = \Delta_2 = 0$). Eigenvalues of the three-level lambda system Hamiltonian are:

$$\lambda_0 = 0 , \quad (1.3a)$$

$$\lambda_+ = \frac{\hbar}{2} \sqrt{\Omega_1^2 + \Omega_2^2} , \quad (1.3b)$$

$$\lambda_- = -\frac{\hbar}{2} \sqrt{\Omega_1^2 + \Omega_2^2} , \quad (1.3c)$$

and the eigenstates corresponding to these eigenvalues are :

$$|\lambda_0\rangle = \frac{\Omega_2}{\sqrt{\Omega_1^2 + \Omega_2^2}} |1\rangle - \frac{\Omega_1}{\sqrt{\Omega_1^2 + \Omega_2^2}} |2\rangle , \quad (1.4a)$$

$$|\lambda_+\rangle = \frac{1}{\sqrt{2}} \left(\frac{\Omega_1}{\sqrt{\Omega_1^2 + \Omega_2^2}} |1\rangle + \frac{\Omega_2}{\sqrt{\Omega_1^2 + \Omega_2^2}} |2\rangle - |3\rangle \right) , \quad (1.4b)$$

$$|\lambda_-\rangle = \frac{1}{\sqrt{2}} \left(\frac{\Omega_1}{\sqrt{\Omega_1^2 + \Omega_2^2}} |1\rangle + \frac{\Omega_2}{\sqrt{\Omega_1^2 + \Omega_2^2}} |2\rangle + |3\rangle \right) . \quad (1.4c)$$

λ_0 is the eigenvalue that corresponds to zero energy state, which is called dark-state and this state $|\lambda_0\rangle$ has zero contribution from bare state $|3\rangle$, meaning if the atom is in state $|\lambda_0\rangle$ possibility of excitation to state $|3\rangle$ is non-existent and since there is no excitation to bare state $|3\rangle$, there will be no radiative decay. Building on this, when the weak probe and strong coupling limit is considered; $\Omega_1 \ll \Omega_2$, dressed states are modified as follows:

$$|\lambda_0\rangle = |1\rangle , \quad (1.5a)$$

$$|\lambda_+\rangle = \frac{1}{\sqrt{2}} (|2\rangle - |3\rangle) , \quad (1.5b)$$

$$|\lambda_-\rangle = \frac{1}{\sqrt{2}} (|2\rangle + |3\rangle) . \quad (1.5c)$$

In the weak probe limit, ground state of the atom becomes the dark-state. There is no contribution from bare states $|2\rangle$ and $|3\rangle$, therefore incident probe light is not absorbed and hence transparency is induced.

In Figure 1.1 comparison of the absorption and refractive index of a three-level lambda system and a two-level system with respect to probe light field detuning is shown. Only difference between the two systems is a coupling light. Blue line represents the two-level system and red line represents the three-level system. In the two-level case when the

probe field is on resonance with the transition, absorption maximum is observed, but in the three-level case absorption diminishes completely on resonance. In the three-level case, energy difference between the dressed-states is $\lambda_+ - \lambda_- = \hbar\Omega_2$ and the absorption spectra shows two absorption peaks symmetric around resonance. Separation between two peaks is $\hbar\Omega_2$. The three-level lambda scheme gives rise to Autler-Townes splitting as well as EIT, separation of dressed-state absorption peaks is called Autler-Townes splitting (Autler and Townes, 1955; Cohen-Tannoudji, 1998). Both effects produce similar absorption spectra and it is often hard to differentiate between them (Abi-Salloum, 2010). Refractive index of the media is also altered for the probe light, with the EIT mechanism. A steep dispersion curve is introduced in a three-level system, causing group velocity for the probe light to decrease.

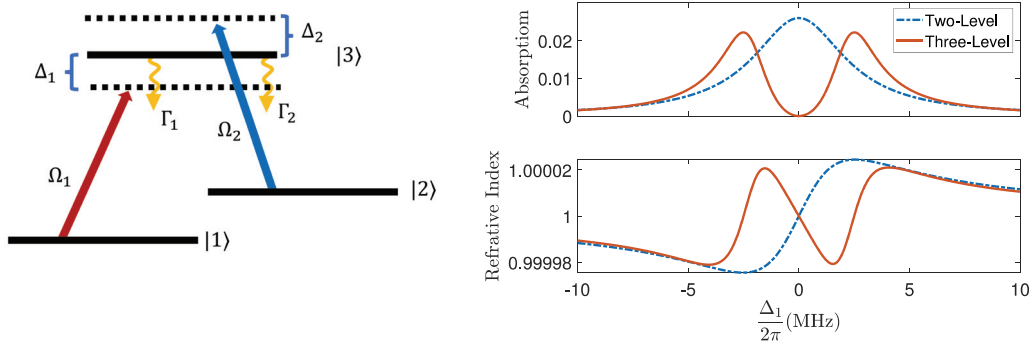


Figure 1.1. **(Left)** Three-level lambda scheme. **(Right - top)** Absorption of the medium for the probe field with respect to different probe field detunings. **(Right - bottom)** Refractive Index of the medium for the probe field with respect to different probe field detunings. Addition of another transition, allows the medium to become transparent for the probe field on resonance.

1.2. Optical Response

In order to understand the optical response of a medium to a light field we need to start from the atomic polarization induced by the light field. Induced atomic polarization by a light field in a medium can be expressed in terms of electric field strength and electric

susceptibility as a power expansion (Boyd, 2008):

$$P = \epsilon_0 [\chi^{(1)}E + \chi^{(2)}E^2 + \chi^{(3)}E^3 + \dots] \quad (1.6)$$

Here ϵ_0 is the permittivity of free space and E is the electric field strength. $\chi^{(1)}$ is the linear electric susceptibility and it describes the linear optical response of the medium. $\chi^{(2)}$ and $\chi^{(3)}$ are the second and third order electric susceptibilities, which describe the non-linear optical response of the medium. Since we are interested in absorption and refractive index, linear optical response term $\chi^{(1)}$ suffices. Induced polarization can also be expressed in terms of expectation value of electric dipole moment:

$$P = N \langle \hat{d} \rangle \quad (1.7)$$

where N is the number density, \hat{d} is the transition dipole operator. When considering three-level lambda scheme; induced polarization includes both probe and coupling light fields' contribution, therefore transition dipole operator includes both transitions. Induced polarization for an atomic medium in a three-level lambda scheme can be written as:

$$P = N [d_{13}\rho_{31} + d_{23}\rho_{32} + c.c.] \quad (1.8)$$

where d_{13} and d_{23} are the transition dipole moments of $|1\rangle \rightarrow |3\rangle$ and $|2\rangle \rightarrow |3\rangle$ transitions and ρ_{31} , ρ_{32} are off diagonal density matrix elements or in other words atomic coherences. Since we are interested in probe light optical properties we consider only $|1\rangle \rightarrow |3\rangle$ transition. Following on that, linear susceptibility for probe light can be written as:

$$\chi = \frac{2Nd_{13}^2}{\epsilon_0\hbar\Omega_1}\rho_{31} \quad (1.9)$$

Imaginary part of this linear susceptibility is directly proportional to the absorption coefficient, therefore transmission for a light field can be acquired from the linear electric susceptibility for that light. Absorption coefficient can be written in terms of linear susceptibility as (Jackson, 1999):

$$\alpha = k_1 \text{Im}[\chi] \quad (1.10)$$

where k_1 is the wavenumber for the probe light and it is defined as: $k_1 = \frac{2\pi}{\lambda_1}$. The relation between transmission of the medium and absorption coefficient is given by Beer-Lambert law:

$$T = e^{-l\alpha} = e^{-lk_1 \text{Im}[\chi]} , \quad (1.11)$$

where l is the length of the medium. Real part of the linear susceptibility is related to an optical property as well. Refractive index of the medium for the light field can be obtained from the real part of linear susceptibility as (Jackson, 1999):

$$n = \sqrt{1 + \text{Re}[\chi]} . \quad (1.12)$$

1.3. Rydberg Atoms

Rydberg atom is an atom which have at least one electron excited to a high principal quantum number n . Rydberg atoms have exaggerated properties such as large size, large dipole moment, long radiative lifetime and extreme sensitivity to electric fields (Gallagher, 1994). For instance atomic radius is given by $n^2 a_0$, where a_0 is the Bohr radius ($a_0 = 0.53 \text{ \AA}$), therefore a Rydberg atom with $n = 100$, has a diameter of $1.06 \mu\text{m}$, so it is possible to say that Rydberg atoms can be macroscopic in size. Large sizes of Rydberg atoms, mean that the distance of the Rydberg state electron to the positive core is very large and this causes a very large dipole moment. Dipole moment scales with principal quantum number as n^2 . Due to large dipole moment very strong interactions between Rydberg atoms are observed. Rydberg atoms also have very long radiative lifetimes, scaling with principal quantum number as n^3 . Table 1.1 shows some of the scaling laws for Rydberg states (Gallagher, 1994).

Rydberg atoms can be created by optical excitation, by means of two-photon excitation where two lasers are employed for exciting atoms from the ground state to a Rydberg state (Gallagher, 1994). Due to Rydberg atoms' high sensitivity to electric fields, Rydberg atoms can be detected by ionization, but this is a destructive process in which the Rydberg state is lost when ionized. With the utility of EIT mechanism configured to include Rydberg states brought up the non-destructive detection and optical spectroscopy

Property	n dependence
Binding Energy	n^{-2}
Orbital Radius	n^2
Dipole Moment	n^2
Radiative Lifetime	n^3
Polarizability	n^7

Table 1.1. Scaling laws of Rydberg state properties with principal quantum number.

of Rydberg states (Mohapatra et al., 2007; Thoumany et al., 2009). Moreover, with Rydberg EIT systems interaction enhanced imaging applications are possible. Exploiting the strong interactions of Rydberg atoms in an EIT configuration cause blockade effect, it is possible to image the Rydberg atoms non-destructively (Günter et al., 2012; Günter et al., 2013; Gavryusev et al., 2016).

Interactions between Rydberg atoms can be of dipolar nature or van der Waals nature. Type of Rydberg-Rydberg interaction depends on the inter-atomic distance. Long-range (several μm) Rydberg-Rydberg interactions are in the van der Waals form. Dipolar Rydberg-Rydberg interaction energy is given by:

$$V_{ij} = \frac{C_3}{|r_i - r_j|^3} . \quad (1.13)$$

Case regarded in this thesis are Rydberg atom interactions in van der Waals form and van der Waals interaction energy is given by:

$$V_{ij} = \frac{C_6}{|r_i - r_j|^6} , \quad (1.14)$$

where C_6 is the van der Waals coefficient and $|r_i - r_j|$ is the distance between i^{th} and j^{th} atoms. C_6 scales with n as n^{11} (Singer et al., 2005). This means that despite the long inter atomic distances, Rydberg atoms interact very strongly with respect to ground state atoms. For instance, two Cesium atoms at $n = 70$ and separated with a distance of $r = 5 \mu m$ produce an interaction energy of 237 MHz. The laser Rabi frequencies utilized

for EIT applications are generally in the range of several tens of MHz and when compared with the Rydberg-Rydberg interaction energies, it is easy to see how strong the interaction is.

Such strong interactions, shift the Rydberg state energy so drastically that, it becomes less probable to excite another atom to a Rydberg state at the same time. An atom excited to a Rydberg state, produces a sphere of influence due to the interaction determined by n and blockade radius r_b . Within this volume of $\frac{4}{3}\pi r_b^3$, it is not possible to excite another atom to a Rydberg state during the lifetime of that Rydberg state. This effect is called Rydberg blockade (Lukin et al., 2001). Rydberg blockade is characterized by r_b and it is determined by the laser's Rabi frequency Ω that facilitates the transition to the Rydberg state. When the interaction energy exceeds Ω , further excitations are blocked. Therefore it is convenient to define the blockade radius at transition resonance as:

$$r_b = \sqrt[6]{\frac{|C_6|}{\Omega}} . \quad (1.15)$$

As an example of how the interaction energy and blockade radius increases with n is shown in Table 1.2 of an ensemble of interacting Cesium atoms separated with an average distance of $5 \mu m$ and with a Rydberg laser Rabi frequency $\Omega = 2\pi \times 0.5$ MHz on resonance. It is possible to see the magnitude of the van der Waals interaction and the respective blockade radii. Therefore it is possible to isolate a Rydberg atom in a very large volume by facilitating the van der Waals interactions.

The Rydberg blockade effect is especially important since it allows for isolating a single excitation to a Rydberg state, therefore enabling Rydberg atoms to be used for studies in quantum many-body physics and quantum information science. Excitation suppression was observed in ultra cold Rydberg atoms due to the blockade effect caused by van der Waals interactions (Tong et al., 2004). Effect of Rydberg atom density on van der Waals interactions and blockade was also studied (Singer et al., 2004). In order to observe Rydberg atom interactions spectroscopically, microwave fields are used to probe the Rydberg state (Afrousheh et al., 2004). Using the blockade mechanism, nature of probability distributions of number of Rydberg excitations in cold ensembles is studied as well (Liebisch et al., 2005). A promising quantum gate application results due to the tunable interactions and blockade of Rydberg atoms (Vogt et al., 2006). It was also demonstrated that, Rydberg blockade can be modulated by applied electric fields due to

n	$V(\text{MHz})$	$r_b(\mu\text{m})$
100	15835.0	20.7036
90	4652.0	16.8805
80	1164.4	13.4007
70	237.8260	10.2838
60	37.1568	7.5472
50	4.0026	5.2060
40	0.2472	3.2731

Table 1.2. van der Waals interaction energies and blockade radii for an ensemble of Cs atoms with an average inter-atomic distance of $5 \mu\text{m}$ and with a Rydberg transition field Rabi frequency of $\Omega = 2\pi \times 0.5 \text{ MHz}$ on resonance. It is clearly seen that the interaction is very strong and even climbing up to 15 GHz at $n = 100$ with a blockade radius of $r_b = 20.7036 \mu\text{m}$.

the induced dipole moment by the field (Vogt et al., 2007). Resonant energy transfer resulting from the Rydberg blockade effect, causing an atom in a volume to excite and simultaneously de-excite another atom in a different volume was demonstrated experimentally (van Ditzhuijzen et al., 2008). Rydberg blockade effects were studied in cold Rubidium atoms with a two-photon excitation scheme (Heidemann et al., 2007) as well as in two-body systems (Urban et al., 2009; Gaëtan et al., 2009).

There are vast number of potential applications that result from the nature of Rydberg atoms such as quantum gates and interaction enhanced imaging. Introduction of Rydberg atoms to EIT configurations allow for the enhancement of non-linear optical effects, but non-linear optical effects are beyond the scope of this thesis. In the next Chapter, theoretical description of a four-level atom-field system will be examined in detail.

CHAPTER 2

THEORY

In this Chapter; EIT mechanism in a four-level ladder scheme will be analyzed as an open system. In Section 2.1, analysis is carried out for a system of non-interacting atoms, after that Rydberg-Rydberg interactions will be considered for a Rydberg EIT system in a semi-classical manner. Firstly, bare Hamiltonian and classical light fields will be defined, followed by the atom-light interaction Hamiltonian derivation. Later, Lindblad superoperator, which includes coupling to environment by radiative decays will be defined. Then Optical Bloch Equations (OBEs) will be solved for steady state probe coherence and analyzed in conjunction with dressed state eigenvalues. Afterwards in Section 2.1.1, system of interacting four-level Rydberg atoms will be considered.

2.1. Three-Photon Electromagnetically Induced Transparency

A system which couples to the environment by dissipation is an open system and open systems evolve with Master Equation (Barnett and Radmore, 2002). Irreversible loss of energy by means of spontaneous emission or radiative decay of excitation requires an open system treatment. EIT with a three-photon excitation scheme, which is the main focus of this thesis, is an open system and requires density matrix formalism and master equation approach. In order to account for the coupling to the environment Lindblad superoperator is used. It includes information on the rate of relaxation and which states are coupled by that decay. Lindblad superoperator can also include laser linewidths, but in scope of this thesis only radiative decays are considered. Master Equation for an N-body system is given as:

$$\dot{\rho}^{(N)} = -\frac{i}{\hbar}[\hat{H}, \rho^{(N)}] + \mathcal{L}[\rho^{(N)}] . \quad (2.1)$$

Here; $\rho^{(N)}$ is the N-body density matrix, \hbar is the Planck's constant, \hat{H} is the total Hamiltonian and $\mathcal{L}[\rho^{(N)}]$ is the Lindblad superoperator. In first part of the Theory Chapter,

we consider the case in which atoms do not interact with one another and later in Rydberg EIT section interacting atoms case is analyzed. For a system where atomic interaction is non-existent, N-body density matrix reduces to single particle density matrix and Master equation can be written as:

$$\dot{\rho} = -\frac{i}{\hbar}[\hat{H}, \rho] + \mathcal{L}[\rho] . \quad (2.2)$$

Resulting equations of motion for non-interacting scenario is regarded as Optical Bloch Equations (OBEs) (Bloch, 1946). In order to acquire OBEs we start with the description of three-photon excitation scheme. In three-photon ladder scheme, atoms in ground state are excited to a subsequent higher energy state via three distinct light fields. States are coupled only by their respective light fields and any other means of transition is not allowed. A level schematic can be seen on Figure 2.1. Ground state is labeled as $|1\rangle$ and the three following excited states are $|2\rangle$, $|3\rangle$ and $|4\rangle$. Excitation to higher energy states are accomplished via light fields represented with their respective Rabi frequencies, Ω_1 , Ω_2 and Ω_3 . Difference between transition frequency and the frequency of the light fields are called detunings, which are shown with Δ_1 , Δ_2 and Δ_3 . Spontaneous decay rates of the states $|2\rangle$, $|3\rangle$ and $|4\rangle$ are represented with Γ_1 , Γ_2 and Γ_3 , respectively.

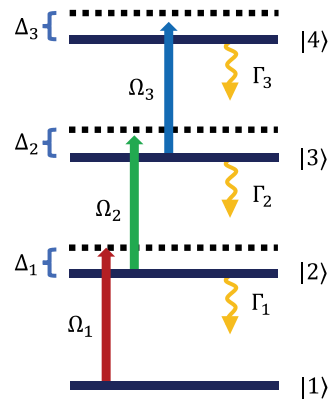


Figure 2.1. Three-photon excitation or four-level ladder scheme. Excitations, $|1\rangle \rightarrow |2\rangle$, $|2\rangle \rightarrow |3\rangle$, $|3\rangle \rightarrow |4\rangle$ are accomplished with three different light fields with Rabi frequencies; Ω_1 , Ω_2 and Ω_3 , respectively. Excited states $|4\rangle$, $|3\rangle$ and $|2\rangle$ have spontaneous decay rates of Γ_3 , Γ_2 and Γ_1 , respectively.

Hamiltonian for a four-level scheme is composed of three parts; bare Hamiltonian \hat{H}_A which contains energies of the atomic states, atom-light interaction Hamiltonian \hat{H}_{AL} and interactions between atoms V :

$$\hat{H} = \hat{H}_A + \hat{H}_{AL} + V . \quad (2.3)$$

At first, non-interacting case is analyzed, therefore we considered $V = 0$ case. Later, in Section 2.1.1, Rydberg-Rydberg interactions are considered and in that Section, V is replaced with V_{ij} for clarity, since pairwise interactions between i^{th} and j^{th} atoms are taken into account.

Bare states are defined in vector form as:

$$|1\rangle = \begin{pmatrix} 1 \\ 0 \\ 0 \\ 0 \end{pmatrix}, \quad |2\rangle = \begin{pmatrix} 0 \\ 1 \\ 0 \\ 0 \end{pmatrix}, \quad |3\rangle = \begin{pmatrix} 0 \\ 0 \\ 1 \\ 0 \end{pmatrix}, \quad |4\rangle = \begin{pmatrix} 0 \\ 0 \\ 0 \\ 1 \end{pmatrix} . \quad (2.4)$$

Bare Hamiltonian is comprised of the sum of atomic state energies and can be written as:

$$\hat{H}_A = E_1 |1\rangle \langle 1| + E_2 |2\rangle \langle 2| + E_3 |3\rangle \langle 3| + E_4 |4\rangle \langle 4| . \quad (2.5)$$

For clarity and easier description we choose our ground state energy to be zero, $E_1 = 0$, then excited state energies are:

$$E_2 = \hbar w_1 , \quad (2.6a)$$

$$E_3 = \hbar(w_1 + w_2) , \quad (2.6b)$$

$$E_4 = \hbar(w_1 + w_2 + w_3) , \quad (2.6c)$$

with w_1, w_2, w_3 being transition frequencies of the states. Then classical light fields are defined with real and complex parts:

$$\mathbf{E}_i(\mathbf{r}, t) = \mathbf{e}_i \frac{1}{2} [\mathcal{E}_i e^{i(\mathbf{k}_i \mathbf{r} - w_{iL} t)} + \mathcal{E}_i^* e^{-i(\mathbf{k}_i \mathbf{r} - w_{iL} t)}] . \quad (2.7)$$

Here; \mathbf{e}_i is the unit polarization vector, \mathcal{E}_i and \mathcal{E}_i^* are the field amplitudes, k_i are the wavenumbers and w_{iL} frequency of the light fields, with $i = 1, 2, 3$. Following that, within dipole approximation atom-light interaction Hamiltonian is defined as the dot product of dipole moment and electric field:

$$\hat{H}_{AL} = -\hat{\mathbf{d}} \cdot \mathbf{E} , \quad (2.8)$$

here $\hat{\mathbf{d}}$ is the dipole moment. In a more explicit form, atom-light interaction Hamiltonian can be written as:

$$\begin{aligned} \hat{H}_{AL} = & \mathbf{d}_{12} \cdot \mathbf{E}_1(\mathbf{r}, t) (|1\rangle \langle 2| + |2\rangle \langle 1|) + \mathbf{d}_{23} \cdot \mathbf{E}_2(\mathbf{r}, t) (|2\rangle \langle 3| + |3\rangle \langle 2|) \\ & + \mathbf{d}_{34} \cdot \mathbf{E}_3(\mathbf{r}, t) (|3\rangle \langle 4| + |4\rangle \langle 3|) , \end{aligned} \quad (2.9)$$

here \mathbf{d}_{ij} are transition dipole moment between i^{th} and j^{th} states and it is defined as $\mathbf{d}_{ij} = \langle i | \hat{\mathbf{d}} | j \rangle$, with dipole operator, $\hat{\mathbf{d}} = -e\hat{\mathbf{r}}$, e being the electric charge and $\hat{\mathbf{r}}$ being the position operator. Combining bare Hamiltonian and atom-light interaction Hamiltonian gives the full Hamiltonian. In the matrix form:

$$\hat{H} = \begin{pmatrix} 0 & \mathbf{d}_{12} \cdot \mathbf{E}_1(\mathbf{r}, t) & 0 & 0 \\ \mathbf{d}_{12} \cdot \mathbf{E}_1(\mathbf{r}, t) & \hbar w_1 & \mathbf{d}_{23} \cdot \mathbf{E}_2(\mathbf{r}, t) & 0 \\ 0 & \mathbf{d}_{23} \cdot \mathbf{E}_2(\mathbf{r}, t) & \hbar(w_1 + w_2) & \mathbf{d}_{34} \cdot \mathbf{E}_3(\mathbf{r}, t) \\ 0 & 0 & \mathbf{d}_{34} \cdot \mathbf{E}_3(\mathbf{r}, t) & \hbar(w_1 + w_2 + w_3) \end{pmatrix} . \quad (2.10)$$

Next, rotating wave approximation (RWA) is required and in order to proceed with RWA transformation to a rotating frame is necessary. Rotating frame Hamiltonian can be acquired by a unitary transformation as:

$$\hat{H}' = \hat{U}^\dagger \hat{H} \hat{U} - i\hbar \hat{U}^\dagger \frac{\partial \hat{U}}{\partial t} . \quad (2.11)$$

Unitary transformation operator \hat{U} is chosen to be:

$$\hat{U} = \begin{pmatrix} 1 & 0 & 0 & 0 \\ 0 & e^{-iw_{1L}t} & 0 & 0 \\ 0 & 0 & e^{-i(w_{1L}+w_{2L})t} & 0 \\ 0 & 0 & 0 & e^{-i(w_{1L}+w_{2L}+w_{3L})t} \end{pmatrix}. \quad (2.12)$$

After carrying out the matrix algebra in Eqn. (2.11), we acquired the rotating frame Hamiltonian:

$$\hat{H}' = \begin{pmatrix} 0 & \mathbf{d}_{12} \cdot \mathbf{E}_1(\mathbf{r}, t) e^{-iw_{1L}t} & 0 & 0 \\ \mathbf{d}_{12} \cdot \mathbf{E}_1(\mathbf{r}, t) e^{iw_{1L}t} & -\hbar\Delta_1 & \mathbf{d}_{23} \cdot \mathbf{E}_2(\mathbf{r}, t) e^{-iw_{2L}t} & 0 \\ 0 & \mathbf{d}_{23} \cdot \mathbf{E}_2(\mathbf{r}, t) e^{iw_{2L}t} & -\hbar(\Delta_1 + \Delta_2) & \mathbf{d}_{34} \cdot \mathbf{E}_3(\mathbf{r}, t) e^{-iw_{3L}t} \\ 0 & 0 & \mathbf{d}_{34} \cdot \mathbf{E}_3(\mathbf{r}, t) e^{iw_{3L}t} & -\hbar(\Delta_1 + \Delta_2 + \Delta_3) \end{pmatrix}. \quad (2.13)$$

Here, we defined the detunings as $\Delta_i = w_{iL} - w_i$ with $i = 1, 2, 3$ and they represent the difference between transition frequency and light field frequency. Following that the next step is to apply RWA, which is eliminating rapidly oscillating terms. In order to determine the rapidly oscillating terms, field vectors need to be written explicitly as follows:

$$\begin{aligned} \mathbf{d}_{12} \cdot \mathbf{E}_1(\mathbf{r}, t) e^{-iw_{1L}t} &= \mathbf{d}_{12} \cdot \mathbf{e}_1 \frac{1}{2} [\mathcal{E}_1 e^{i(\mathbf{k}_1 \mathbf{r} - w_{1L}t)} + \mathcal{E}_1^* e^{-i(\mathbf{k}_1 \mathbf{r} - w_{1L}t)}] e^{-iw_{1L}t}, \\ \mathbf{d}_{12} \cdot \mathbf{E}_1(\mathbf{r}, t) e^{-iw_{1L}t} &= \mathbf{d}_{12} \cdot \mathbf{e}_1 \frac{1}{2} [\mathcal{E}_1 e^{i(\mathbf{k}_1 \mathbf{r} - 2w_{1L}t)} + \mathcal{E}_1^* e^{-i(\mathbf{k}_1 \mathbf{r})}], \\ \mathbf{d}_{12} \cdot \mathbf{E}_1(\mathbf{r}, t) e^{-iw_{1L}t} &= \mathbf{d}_{12} \cdot \mathbf{e}_1 \frac{\mathcal{E}_1^* e^{-i\mathbf{k}_1 \mathbf{r}}}{2}. \end{aligned} \quad (2.14)$$

Here rapidly oscillating term is $e^{-i2w_{1L}t}$ and it can be neglected so we are left with Eqn. (2.14). Same straightforward cancellation is performed for every transition dipole moment and field product terms and Hamiltonian within RWA becomes:

$$\hat{H}' = \hbar \begin{pmatrix} 0 & \frac{\mathbf{d}_{12} \cdot \mathbf{e}_1}{2\hbar} \mathcal{E}_1^* e^{-i\mathbf{k}_1 \mathbf{r}} & 0 & 0 \\ \frac{\mathbf{d}_{12} \cdot \mathbf{e}_1}{2\hbar} \mathcal{E}_1 e^{i\mathbf{k}_1 \mathbf{r}} & -\Delta_1 & \frac{\mathbf{d}_{23} \cdot \mathbf{e}_2}{2\hbar} \mathcal{E}_2^* e^{-i\mathbf{k}_2 \mathbf{r}} & 0 \\ 0 & \frac{\mathbf{d}_{23} \cdot \mathbf{e}_2}{2\hbar} \mathcal{E}_2 e^{i\mathbf{k}_2 \mathbf{r}} & -\Delta_1 - \Delta_2 & \frac{\mathbf{d}_{34} \cdot \mathbf{e}_3}{2\hbar} \mathcal{E}_3^* e^{-i\mathbf{k}_3 \mathbf{r}} \\ 0 & 0 & \frac{\mathbf{d}_{34} \cdot \mathbf{e}_3}{2\hbar} \mathcal{E}_3 e^{i\mathbf{k}_3 \mathbf{r}} & -\Delta_1 - \Delta_2 - \Delta_3 \end{pmatrix}, \quad (2.15)$$

in which real and complex Rabi frequencies are defined as $\Omega_i = \frac{\mathbf{d}_{ij} \cdot \mathbf{e}_i}{\hbar} \mathcal{E}_i e^{i\mathbf{k}_i \mathbf{r}}$, with $i = 1, 2, 3$. If we assume that the Rabi frequencies are real, $\Omega_i = \Omega_i^*$, then final form of the Hamiltonian in matrix form is written as:

$$\hat{H}' = \hbar \begin{pmatrix} 0 & \frac{\Omega_1}{2} & 0 & 0 \\ \frac{\Omega_1}{2} & -\Delta_1 & \frac{\Omega_2}{2} & 0 \\ 0 & \frac{\Omega_2}{2} & -\Delta_1 - \Delta_2 & \frac{\Omega_3}{2} \\ 0 & 0 & \frac{\Omega_3}{2} & -\Delta_1 - \Delta_2 - \Delta_3 \end{pmatrix}. \quad (2.16)$$

After obtaining the Hamiltonian for the system, now we need to define density matrix and dissipation terms for equations of motion. Since the system has four atomic states, single particle density matrix can be written as a 4x4 matrix, in which the diagonal elements represent the state populations and off-diagonal elements represent the coherences,

$$\rho = \begin{pmatrix} \rho_{11} & \rho_{12} & \rho_{13} & \rho_{14} \\ \rho_{21} & \rho_{22} & \rho_{23} & \rho_{24} \\ \rho_{31} & \rho_{32} & \rho_{33} & \rho_{34} \\ \rho_{41} & \rho_{42} & \rho_{43} & \rho_{44} \end{pmatrix}. \quad (2.17)$$

Lindblad superoperator, which describes the dissipation of the system to the environment in the most general form is given as:

$$\mathcal{L}[\rho] = \sum_{k=1}^3 \Gamma_k \left[L_k \rho L_k^\dagger - \frac{1}{2} L_k^\dagger L_k \rho - \frac{1}{2} \rho L_k^\dagger L_k \right], \quad (2.18)$$

where, $L_1 = \hat{\sigma}_{12}$, $L_2 = \hat{\sigma}_{23}$ and $L_3 = \hat{\sigma}_{34}$, with $\hat{\sigma}_{ij} = |i\rangle \langle j|$ being the atomic transition operators. Since the three-photon excitation scheme includes three decay channels $\Gamma_1, \Gamma_2, \Gamma_3$ there are three terms in Lindblad superoperator:

$$\mathcal{L}[\rho] = \mathcal{L}_{21}[\rho] + \mathcal{L}_{32}[\rho] + \mathcal{L}_{43}[\rho], \quad (2.19a)$$

$$\mathcal{L}_{21}[\rho] = \Gamma_1 \begin{pmatrix} \rho_{22} & -\frac{\rho_{12}}{2} & 0 & 0 \\ -\frac{\rho_{21}}{2} & -\rho_{22} & -\frac{\rho_{23}}{2} & -\frac{\rho_{24}}{2} \\ 0 & -\frac{\rho_{32}}{2} & 0 & 0 \\ 0 & -\frac{\rho_{42}}{2} & 0 & 0 \end{pmatrix}, \quad (2.19b)$$

$$\mathcal{L}_{32}[\rho] = \Gamma_2 \begin{pmatrix} 0 & 0 & -\frac{\rho_{13}}{2} & 0 \\ 0 & \rho_{33} & -\frac{\rho_{23}}{2} & 0 \\ -\frac{\rho_{31}}{2} & -\frac{\rho_{32}}{2} & -\rho_{33} & -\frac{\rho_{34}}{2} \\ 0 & 0 & -\frac{\rho_{43}}{2} & 0 \end{pmatrix}, \quad (2.19c)$$

$$\mathcal{L}_{43}[\rho] = \Gamma_3 \begin{pmatrix} 0 & 0 & 0 & -\frac{\rho_{14}}{2} \\ 0 & 0 & 0 & -\frac{\rho_{24}}{2} \\ 0 & 0 & \rho_{44} & -\frac{\rho_{34}}{2} \\ -\frac{\rho_{41}}{2} & -\frac{\rho_{42}}{2} & -\frac{\rho_{43}}{2} & -\rho_{44} \end{pmatrix}. \quad (2.19d)$$

Following that, the resulting equations of motion or OBEs from Eqn. (2.2) for a four-level ladder scheme, are as follows:

$$\frac{d}{dt}\rho_{11} = \frac{i}{2}\Omega_1(\rho_{12} - \rho_{21}) + \Gamma_1\rho_{22} \quad (2.20a)$$

$$\frac{d}{dt}\rho_{22} = -\frac{i}{2}\Omega_1(\rho_{12} - \rho_{21}) + \frac{i}{2}\Omega_2(\rho_{23} - \rho_{32}) + \Gamma_2\rho_{33} - \Gamma_1\rho_{22} \quad (2.20b)$$

$$\frac{d}{dt}\rho_{33} = -\frac{i}{2}\Omega_2(\rho_{23} - \rho_{32}) + \frac{i}{2}\Omega_3(\rho_{34} - \rho_{43}) + \Gamma_3\rho_{44} - \Gamma_2\rho_{33} \quad (2.20c)$$

$$\frac{d}{dt}\rho_{44} = -\frac{i}{2}\Omega_3(\rho_{34} - \rho_{43}) - \Gamma_3\rho_{44} \quad (2.20d)$$

$$\frac{d}{dt}\rho_{12} = \frac{i}{2}\Omega_1(\rho_{11} - \rho_{22}) + \frac{i}{2}\Omega_2\rho_{13} - i\Delta_1\rho_{12} - \frac{\Gamma_1}{2}\rho_{12} \quad (2.20e)$$

$$\frac{d}{dt}\rho_{13} = \frac{i}{2}\Omega_3\rho_{14} + \frac{i}{2}\Omega_2\rho_{12} - \frac{i}{2}\Omega_1\rho_{23} - i(\Delta_1 + \Delta_2)\rho_{13} - \frac{\Gamma_2}{2}\rho_{13} \quad (2.20f)$$

$$\frac{d}{dt}\rho_{14} = \frac{i}{2}\Omega_3\rho_{13} - \frac{i}{2}\Omega_1\rho_{24} - i(\Delta_1 + \Delta_2 + \Delta_3)\rho_{14} - \frac{\Gamma_3}{2}\rho_{14} \quad (2.20g)$$

$$\frac{d}{dt}\rho_{23} = \frac{i}{2}\Omega_2(\rho_{22} - \rho_{33}) - \frac{i}{2}\Omega_1\rho_{13} + i\frac{\Omega_3}{2}\rho_{24} - i\Delta_2\rho_{23} - \frac{(\Gamma_1 + \Gamma_2)}{2}\rho_{23} \quad (2.20h)$$

$$\frac{d}{dt}\rho_{24} = \frac{i}{2}\Omega_3\rho_{23} - \frac{i}{2}\Omega_2\rho_{34} - \frac{i}{2}\Omega_1\rho_{14} - i(\Delta_2 + \Delta_3)\rho_{24} - \frac{(\Gamma_1 + \Gamma_3)}{2}\rho_{24} \quad (2.20i)$$

$$\frac{d}{dt}\rho_{34} = \frac{i}{2}\Omega_3(\rho_{33} - \rho_{44}) - \frac{i}{2}\Omega_2\rho_{24} - i\Delta_3\rho_{34} - \frac{(\Gamma_2 + \Gamma_3)}{2}\rho_{34} \quad (2.20j)$$

with the condition,

$$\dot{\rho}_{11} + \dot{\rho}_{22} + \dot{\rho}_{33} + \dot{\rho}_{44} = 0. \quad (2.21)$$

We first analyzed the optical response of the atomic medium for the steady state case. In steady state, system does not evolve in time or mathematically, time derivatives in Eqn. (2.20) are zero. In order to observe the optical response of the system, OBEs are solved for probe coherence ρ_{12} for steady state.

Figure 2.2 shows the graph of imaginary part and real part of probe coherence ρ_{12} with respect to detuning of the probe field Δ_1 for a four-level ladder scheme. Parameters used are taken from the article (Šibalić et al., 2016). Rabi frequencies of the light fields are: $\Omega_1 = 2\pi \times 0.1$ MHz, $\Omega_2 = 2\pi \times 8$ MHz, $\Omega_3 = 2\pi \times 0.5$ MHz. Atomic state decay rates are: $\Gamma_3 = 0$ MHz, $\Gamma_2 = \Gamma_1 = 2\pi \times 1$ MHz. Light field detunings are: $\Delta_2 = 0$ MHz, $\Delta_3 = -2\pi \times 4$ MHz. In the top part of the Figure, imaginary part of probe coherence with respect to probe detuning is shown. Narrow EIT feature can be observed at three-photon resonance $\Delta_1 + \Delta_2 + \Delta_3 = 0$. The absorptive peak observed at $\Delta_1 = -2\pi \times 4$ MHz is the absorption of one of the dressed states formed by the strong dressing field Ω_2 and it is due to Autler-Townes splitting. The other absorption peak caused by Autler-Townes splitting is at three-photon resonance $\Delta_1 = -2\pi \times 4$ MHz, but an EIT window occurs there, meaning the other dressed state is transparent for the probe field. In other words, with the four-level ladder system and with a strong dressing field Ω_2 , a dark state forms at three-photon resonance and the dark state results in a transparency window for the probe field. Bottom part of Figure 2.2 shows the dispersive properties for the probe field with respect to probe detuning. At the three-photon resonance, a steep dispersion curve is observed, this causes the group velocity of light to reduce. MATLAB script used in production of this figure is provided in Section A.1.

Figure 2.3 shows the comparison of eigenvalues of the system and imaginary part of probe coherence with respect to probe field detuning. Top part of Figure 2.3 shows the eigenvalues of system Hamiltonian in Eqn. (2.16) with respect to probe detuning. Middle part shows imaginary part of probe coherence with respect to probe detuning, it is the zoomed in version of Figure 2.2 around three-photon resonance where the EIT behavior is observed. Black horizontal dashed line is $y = 0$ line and it indicates the zero eigenvalues. Grey vertical lines indicate the points where avoided crossings occur. Avoided crossings signify excitations and for excitation to occur photons are needed to be absorbed. These avoided crossings correspond exactly to the two absorption peaks around EIT. Moreover, at the region around three-photon resonance $\Delta_1 = 2\pi \times 4$ MHz, eigenvalue λ_3 is zero. A zero eigenvalue means a dark-state is formed and no absorption for the probe field should be present. Therefore at three-photon resonance induced transparency is observed.

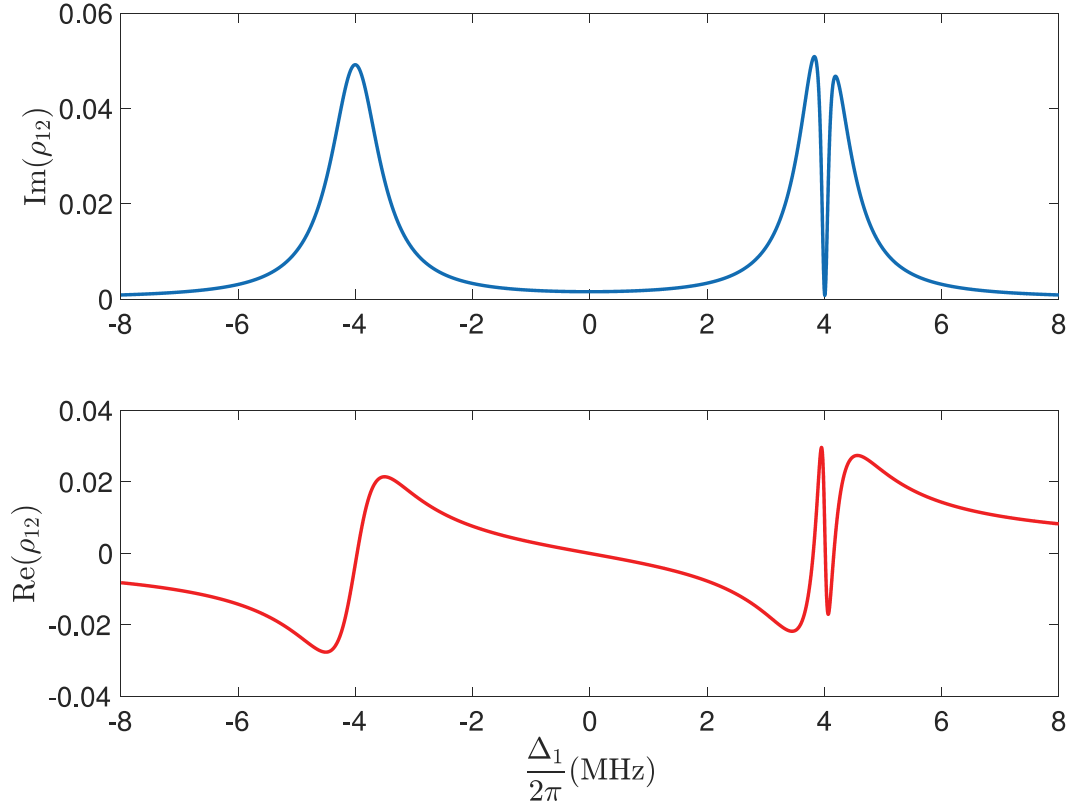


Figure 2.2. **(Top)** Imaginary part and **(Bottom)** real part of probe coherence, with respect to detuning of the probe field for a four-level ladder system in steady state. The dip occurring at the three-photon resonance frequency $\Delta_1 = 2\pi \times 4$ represents the vanishing of absorption in the medium. At the frequency where EIT is observed, steep dispersion curve or rapid change in refractive index is observed (Šibalić et al., 2016). Other parameters are provided in text.

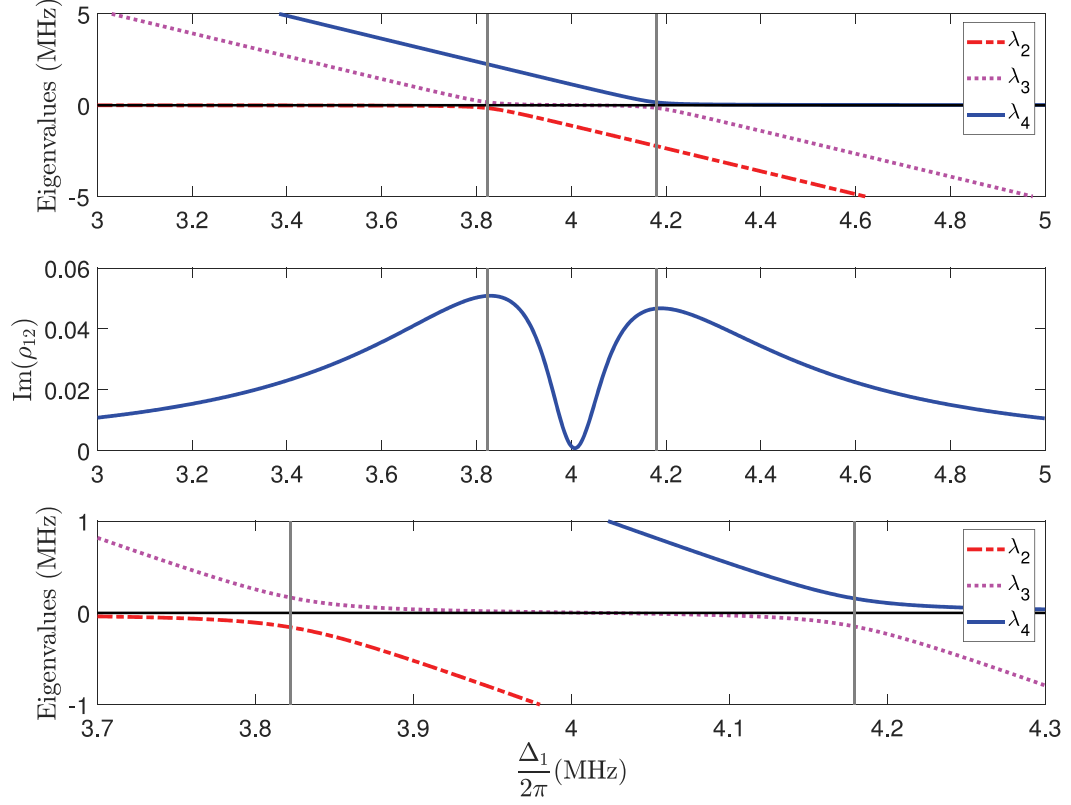


Figure 2.3. **(Top)** Eigenvalues for the system Hamiltonian of four-level scheme with respect to probe field detuning. **(Middle)** Imaginary part of probe coherence with respect to probe field detuning. **(Bottom)** Zoomed in avoided eigenvalue crossings. Grey vertical lines indicate avoided crossing frequencies. Avoided crossings correspond exactly to the absorption maxima. A dark-state or zero eigenvalue corresponds to the EIT window that occurs around three-photon resonance $\Delta_1 = 2\pi \times 4$ MHz. Parameters are the same as in Figure 2.2

2.1.1. Electromagnetically Induced Transparency with Interacting Rydberg Atoms

In Rydberg EIT, the highest state in four-level ladder scheme shown in Figure 2.1 is a Rydberg state. With a Rydberg state included in the scheme, Rydberg atom interaction effects on EIT features of the system can be studied, since Rydberg blockade affects excitation to Rydberg state, therefore changing the optical response (Weatherill et al., 2008). Rydberg atom interactions are considered in the form of van der Waals interactions. Recalling the many body master equation in Eqn. (2.1) with Hamiltonian as in Eqn. (2.3), van der Waals interaction term is in $V_{ij} = \frac{C_6}{|r_i - r_j|^6}$ form. In the interaction terms, pairwise interactions are considered between i^{th} and j^{th} atoms and $|r_i - r_j|$ is the distance between i^{th} and j^{th} atoms.

For a system composed of four levels, many-body equations of motion become:

$$\frac{d}{dt}\rho_{11}^{(i)} = \frac{i}{2}\Omega_1 (\rho_{12}^{(i)} - \rho_{21}^{(i)}) + \Gamma_1\rho_{22}^{(i)} \quad (2.22a)$$

$$\frac{d}{dt}\rho_{22}^{(i)} = -\frac{i}{2}\Omega_1 (\rho_{12}^{(i)} - \rho_{21}^{(i)}) + \frac{i}{2}\Omega_2 (\rho_{23}^{(i)} - \rho_{32}^{(i)}) + \Gamma_2\rho_{33}^{(i)} - \Gamma_1\rho_{22}^{(i)} \quad (2.22b)$$

$$\frac{d}{dt}\rho_{33}^{(i)} = -\frac{i}{2}\Omega_2 (\rho_{23}^{(i)} - \rho_{32}^{(i)}) + \frac{i}{2}\Omega_3 (\rho_{34}^{(i)} - \rho_{43}^{(i)}) + \Gamma_3\rho_{44}^{(i)} - \Gamma_2\rho_{33}^{(i)} \quad (2.22c)$$

$$\frac{d}{dt}\rho_{44}^{(i)} = -\frac{i}{2}\Omega_3 (\rho_{34}^{(i)} - \rho_{43}^{(i)}) - \Gamma_3\rho_{44}^{(i)} \quad (2.22d)$$

$$\frac{d}{dt}\rho_{12}^{(i)} = \frac{i}{2}\Omega_1 (\rho_{11}^{(i)} - \rho_{22}^{(i)}) + \frac{i}{2}\Omega_2\rho_{13}^{(i)} - i\Delta_1\rho_{12}^{(i)} - \frac{\Gamma_1}{2}\rho_{12}^{(i)} \quad (2.22e)$$

$$\frac{d}{dt}\rho_{13}^{(i)} = \frac{i}{2}\Omega_3\rho_{14}^{(i)} + \frac{i}{2}\Omega_2\rho_{12}^{(i)} - \frac{i}{2}\Omega_1\rho_{23}^{(i)} - i(\Delta_1 + \Delta_2)\rho_{13}^{(i)} - \frac{\Gamma_2}{2}\rho_{13}^{(i)} \quad (2.22f)$$

$$\frac{d}{dt}\rho_{14}^{(i)} = \frac{i}{2}\Omega_3\rho_{13}^{(i)} - \frac{i}{2}\Omega_1\rho_{24}^{(i)} - i(\Delta_1 + \Delta_2 + \Delta_3)\rho_{14}^{(i)} - \frac{\Gamma_3}{2}\rho_{14}^{(i)} + i \sum_{i \neq j} V_{ij}\rho_{14,44}^{(i,j)} \quad (2.22g)$$

$$\frac{d}{dt}\rho_{23}^{(i)} = \frac{i}{2}\Omega_2 (\rho_{22}^{(i)} - \rho_{33}^{(i)}) - \frac{i}{2}\Omega_1\rho_{13}^{(i)} + \frac{\Omega_3}{2}\rho_{24}^{(i)} - i\Delta_2\rho_{23}^{(i)} - \frac{(\Gamma_1 + \Gamma_2)}{2}\rho_{23}^{(i)} \quad (2.22h)$$

$$\frac{d}{dt}\rho_{24}^{(i)} = \frac{i}{2}\Omega_3\rho_{23}^{(i)} - \frac{i}{2}\Omega_2\rho_{34}^{(i)} - \frac{i}{2}\Omega_1\rho_{14}^{(i)} - i(\Delta_2 + \Delta_3)\rho_{24}^{(i)} - \frac{(\Gamma_1 + \Gamma_3)}{2}\rho_{24}^{(i)} \quad (2.22i)$$

$$+ i \sum_{i \neq j} V_{ij}\rho_{24,44}^{(i,j)}$$

$$\frac{d}{dt}\rho_{34}^{(i)} = \frac{i}{2}\Omega_3 (\rho_{33}^{(i)} - \rho_{44}^{(i)}) - \frac{i}{2}\Omega_2\rho_{24}^{(i)} - i\Delta_3\rho_{34}^{(i)} - \frac{(\Gamma_2 + \Gamma_3)}{2}\rho_{34}^{(i)} \quad (2.22j)$$

$$+ i \sum_{i \neq j} V_{ij}\rho_{34,44}^{(i,j)}$$

Here $\rho_{\alpha\beta,\theta\gamma}^{(i,j)}$ are two-body density matrices and subscripts $\alpha, \beta, \theta, \gamma$ are atomic

states. Rabi frequencies and detunings for an many-body system may vary among atoms, but we assumed that, Rabi frequencies and detunings are exactly the same for each and every atom, $\Omega_i^{(i)} = \Omega_i$ and $\Delta_i^{(i)} = \Delta_i$. Coherences, which involve the 4th state or Rydberg state, are modified with the inclusion of two-body density matrix terms. Without any interaction present in the system, these terms will disappear and many-body equations of motion will reduce to single particle OBEs as in Eqn. (2.2). In order to solve many-body equations of motion, two-body density matrices are needed. But equations of motion of two-body density matrices involve three-body density matrices and equations of motion of three-body density matrices involve four-body density matrices and this type of hierarchy persists. Therefore it is impossible to exactly solve a system of equations such as this one (Schempp et al., 2010). There are possible approaches to account for interacting many-body case. One of the possible solutions to this problem is the mean-field approach, where two-body density matrices are approximated to product of single-body density matrices and correlations are neglected. There are a number of studies which employ the mean-field method in Rydberg EIT scenarios (Tong et al., 2004; Weimer et al., 2008; Chotia et al., 2008). One other possibility of truncating this hierarchy is reduced density matrix approach (Sevinçli et al., 2011; Schempp et al., 2010). Rate equation model is also used to analyze many-body Rydberg schemes. In this model, many-body equations of motion are transformed to rate equations for population, followed by Monte-Carlo sampling to solve the problem (Ates et al., 2006, 2007; Lesanovsky et al., 2010; Sevinçli et al., 2011; Ates et al., 2011). In this thesis, in order to overcome this problem we tried two different methods. In the first one, we used mean-field method in which we reduce the two-body density matrices to single-body density matrices by $\rho_{\alpha\beta,\theta\gamma}^{(i,j)} = \rho_{\alpha\beta}^{(i)}\rho_{\theta\gamma}^{(j)}$. Here $\alpha, \beta, \theta, \gamma$ are the atomic states and i, j are indices that represent different atoms. As a second method, we used rate equation model.

In the next chapter, mean-field method is explained in detail, followed by application to the simplest case of two-body system. Later, self-consistent mean-field method for larger systems is developed and results are presented.

CHAPTER 3

MEAN-FIELD APPROACH

In this chapter mean-field approach is used firstly, for a very simple case of two identical interacting atoms. Two-body case is considered because of its simplicity which allows for a more in-depth analysis of Rydberg interaction effects. In the two-body case, only factors affecting the interaction strength are inter-atomic distance and principal quantum number, therefore this case enables a more controlled observation of Rydberg-Rydberg interaction effects. Following that, we increased the complexity by increasing the number of atoms in the system and in order to achieve more realistic results by increasing accuracy of the solution, we employed a self-consistent mean-field algorithm.

3.1. Mean-Field Approximation

As discussed earlier, it is not possible to exactly evaluate the equations of motion of two-body density matrices, since they involve three-body density matrices and equations of motion of three-body density matrices involve four-body density matrices and so on, therefore we used the mean-field approach in order to truncate the hierarchy of density matrices. With the mean-field method, it is possible to write two-body density matrices as a product of single-body density matrices. This simplification of many-body density matrices make the problem solvable. Under mean-field approximation, two-body density matrices can be written as:

$$\rho_{\alpha\beta,\theta\gamma}^{(i,j)} = \rho_{\alpha\beta}^{(i)} \rho_{\theta\gamma}^{(j)} . \quad (3.1)$$

Here atomic states are represented by subscripts; $\alpha, \beta, \theta, \gamma$. Superscripts i and j refer to different atoms which are interacting. Equations of motion are modified due to van der Waals interaction within mean-field approximation and below Equation (3.2) shows only 3 out of 6 equations that are modified, since the other 3 equations are simply the conjugates of shown equations $\dot{\rho}_{\alpha\beta}^{(i)} = \left(\dot{\rho}_{\alpha\beta}^{(i)} \right)^* = \dot{\rho}_{\beta\alpha}^{(i)}$.

$$\begin{aligned} \frac{d}{dt}\rho_{14}^{(i)} &= \frac{i}{2}\Omega_3\rho_{13}^{(i)} - \frac{i}{2}\Omega_1\rho_{24}^{(i)} - i(\Delta_1 + \Delta_2 + \Delta_3)\rho_{14}^{(i)} - \frac{\Gamma_3}{2}\rho_{14}^{(i)} \\ &+ i \sum_{i \neq j} V_{ij}\rho_{14}^{(i)}\rho_{44}^{(j)} \quad , \end{aligned} \quad (3.2a)$$

$$\begin{aligned} \frac{d}{dt}\rho_{24}^{(i)} &= \frac{i}{2}\Omega_3\rho_{23}^{(i)} - \frac{i}{2}\Omega_2\rho_{34}^{(i)} - \frac{i}{2}\Omega_1\rho_{14}^{(i)} - i(\Delta_2 + \Delta_3)\rho_{24}^{(i)} - \frac{(\Gamma_1 + \Gamma_3)}{2}\rho_{24}^{(i)} \\ &+ i \sum_{i \neq j} V_{ij}\rho_{24}^{(i)}\rho_{44}^{(j)} \quad , \end{aligned} \quad (3.2b)$$

$$\begin{aligned} \frac{d}{dt}\rho_{34}^{(i)} &= \frac{i}{2}\Omega_3 \left(\rho_{33}^{(i)} - \rho_{44}^{(i)} \right) - \frac{i}{2}\Omega_2\rho_{24}^{(i)} - i\Delta_3\rho_{34}^{(i)} - \frac{(\Gamma_2 + \Gamma_3)}{2}\rho_{34}^{(i)} \\ &+ i \sum_{i \neq j} V_{ij}\rho_{34}^{(i)}\rho_{44}^{(j)} \quad . \end{aligned} \quad (3.2c)$$

3.1.1. Two-Body System

The most simple case to understand EIT effects with mean-field approach is to apply it to an interacting two-body system. In this case, the atomic positions are irrelevant and only quantities affecting the interaction between them are; principle quantum number and inter-atomic distance.

We consider a case of two interacting cesium atoms, with the state configuration: $6S_{1/2} \rightarrow 6P_{3/2} \rightarrow 7S_{1/2} \rightarrow nP$. After we obtain equations of motion for the system, we used MATLAB to solve this system of equations for steady state. But firstly, we needed to check the time evolution of populations and imaginary and real parts of probe coherence in order to find out how long it takes for the system to evolve and reach a steady state. Time it takes for the system to reach steady state determines at what time value the software will solve the coupled differential equations, therefore it affects the computation time as well as the accuracy of the solution.

Figure 3.1 shows the time evolution of ground state and Rydberg state populations, imaginary part and real part of probe coherence ρ_{12} for a two-body system with inter-atomic distance of $5 \mu m$. It is clear that, for this case system reaches to a steady state at $10 \mu s$. System parameters (in units of MHz) used to obtain time evolution Figure 3.1 are: $n = 60$, $r = 5 \mu m$, $\Omega_1 = 2\pi \times 0.1$, $\Omega_2 = 2\pi \times 8$, $\Omega_3 = 2\pi \times 1$, $\Gamma_1 = 2\pi \times 5.39$, $\Gamma_2 = 2\pi \times 3.31$, $\Gamma_3 = 0$, $\Delta_1 = 2\pi \times 4$, $\Delta_2 = 0$, $\Delta_3 = -2\pi \times 4$. We preferred to check the steady state time at three-photon resonance $\Delta_1 + \Delta_2 + \Delta_3 = 0$ since EIT effect is

prominent at three-photon resonance. We chose $\Gamma_3 = 0$, because radiative lifetime of the Rydberg state is three orders of magnitude higher than radiative lifetimes of $6P_{3/2}$ and $7S_{1/2}$ states, since radiative lifetime scales with n as n^3 .

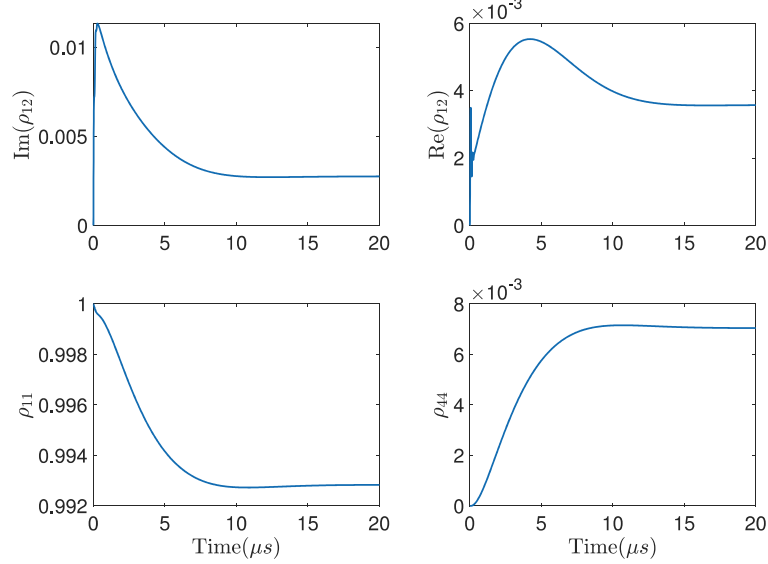


Figure 3.1. Evolution of ground state, Rydberg state populations and imaginary and real parts of probe coherence ρ_{12} with respect to time. Time evolution for three-photon resonance $\Delta_1 = 2\pi \times 4$ MHz is shown because EIT window is observed at three-photon resonance. Other parameters are provided in text.

Distance between two atoms are chosen to be $r = 5 \mu m$, since at $n = 60$, blockade radius is $r_b = 5.31 \mu m$, meaning that atoms are inside the blockade region. Table 3.1 shows blockade radii and van der Waals interaction energies for different n calculated using the same parameters as in Figure 3.1. This table is different than Table 1.3, since we did not assume resonance condition here. When there is a detuning blockade radius in Eqn. 1.15 is no longer valid. With the presence of a detuning on coupling field, blockade radius is modified as follows:

$$r_b = \sqrt[6]{\frac{|C_6|}{\Omega_{3_{eff}}^2}}, \quad (3.3)$$

here $\Omega_{3_{eff}}$ is the effective Rabi frequency and it is defined as $\Omega_{3_{eff}} = \sqrt{\Omega_3^2 + \Delta_3^2}$.

n	$V(\text{MHz})$	$r_b(\mu\text{m})$
100	15835.0	14.56
90	4652.0	11.87
80	1164.4	9.43
70	237.8260	7.23
60	37.1568	5.31
50	4.0026	3.66

Table 3.1. van der Waals interaction energies and blockade radii for two interacting Cs atoms for different n . Other parameters are provided in text.

After analyzing time evolution, imaginary and real parts of probe coherence are calculated with respect to probe field detuning at different principal quantum numbers while keeping the inter-atomic distance constant, in order to observe the effect of van der Waals interaction on EIT. Ground state and Rydberg state populations with respect to probe detuning were also calculated as well. Moreover we performed another calculation to see the effect of inter-atomic distance on EIT. As the atoms get closer to one another, van der Waals interaction increases and disrupts the EIT effect. For distance calculations, principal quantum number kept constant at $n = 60$. Ground state, Rydberg state populations, imaginary part and real part of probe coherence are calculated. Parameters except for n and r , used in following calculations are as follows (in MHz): $\Omega_1 = 2\pi \times 0.1$, $\Omega_2 = 2\pi \times 8$, $\Omega_3 = 2\pi \times 1$, $\Gamma_1 = 2\pi \times 5.39$, $\Gamma_2 = 2\pi \times 3.31$, $\Gamma_3 = 0$, $\Delta_2 = 0$, $\Delta_3 = -2\pi \times 4$. For the calculations where effect of n is investigated, inter-atomic distance is kept constant at $r = 5 \mu\text{m}$ and for the calculations where the effect of r is investigated, principal quantum number is kept constant at $n = 60$.

Figure 3.2 shows imaginary part of probe coherence with respect to probe detuning, for changing n , with $r = 5 \mu\text{m}$. Inset shows the region around three-photon resonance for clarity. EIT window occurs at three-photon resonance $\Delta_1 = 2\pi \times 4$ MHz and as the interaction gets stronger by means of increasing n , EIT window starts to shift

away from three-photon resonance and transparency weakens. From Table 3.1, at $n = 50$ blockade radius is $3.66 \mu m$ and inter-atomic distance is $5 \mu m$, meaning that interaction does not disturb the excitation of the second atom to Rydberg state, therefore EIT mechanism persists. But as can be seen from the inset; starting from $n = 60$ EIT behavior start to change since blockade radius at $n = 60$ is $5.31 \mu m$, meaning atoms are inside the blocked region. As the interaction gets stronger, probability of exciting both atoms to a Rydberg state decreases and transparency fades.

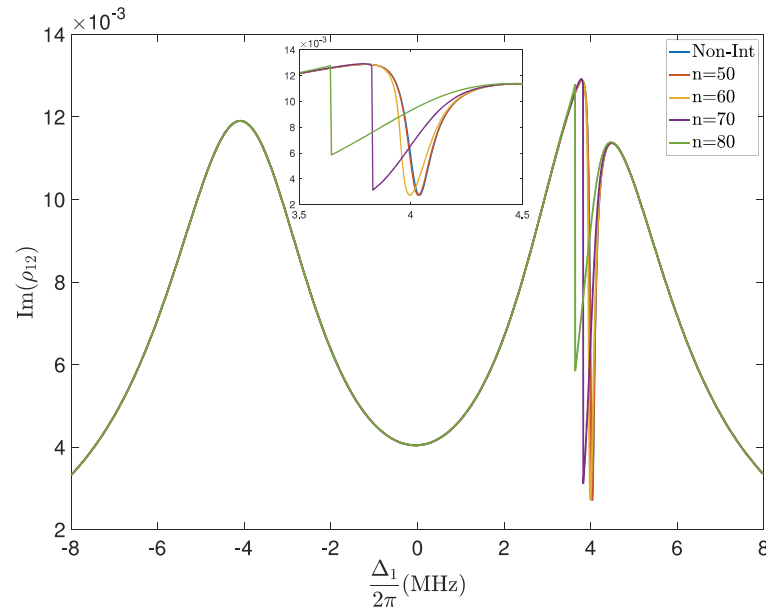


Figure 3.2. Imaginary part of probe coherence with $r = 5 \mu m$ at different n , with respect to probe field detuning. Inset shows the region around three-photon resonance ($\Delta_1 = 2\pi \times 4$ MHz). Other parameters are provided in text.

Figure 3.3, shows imaginary part of probe coherence, with respect to probe detuning, for changing r with $n = 60$. Cases of $r = 1, 2, 4, 6 \mu m$ with $n = 60$ are shown. Inset shows the region around three-photon resonance for clarity. Recalling the van der Waals interaction definition in Eqn. (1.14), as the inter-atomic distance decreases, van der Waals interaction increases. From Table 3.1, at $n = 60$, blockade radius is $5.31 \mu m$, therefore when the inter-atomic distance is larger than blockade radius van der Waals interaction does not affect the mechanism of EIT, but when the atomic separation becomes smaller than blockade radius, interaction shows its effect. When the atoms are inside the blockade

region, excitation to Rydberg state is not possible at the same instance. This in turn effects the formation of EIT. As the atoms get closer to one another, interaction increases and in the case of $r = 1 \mu m$, transparency is completely lost and the system is now an effective three-level system.

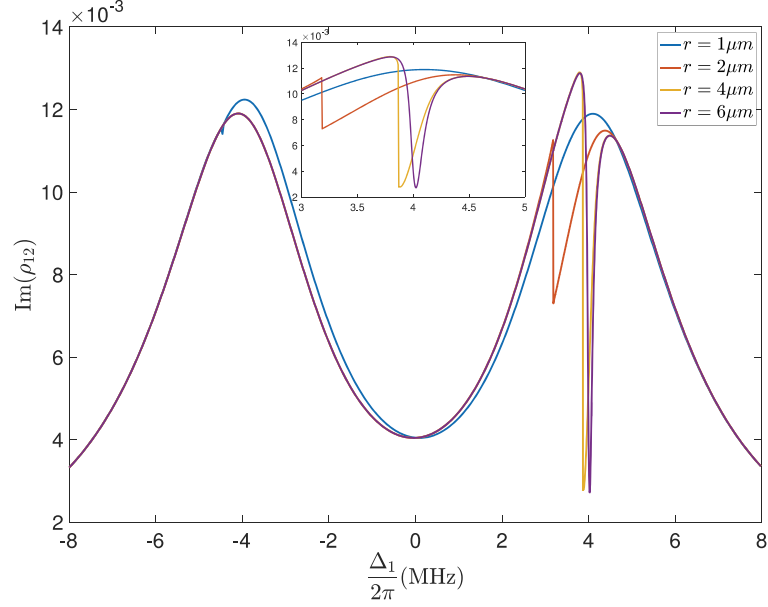


Figure 3.3. Imaginary part of probe coherence at $n = 60$, with different r , with respect to probe field detuning. Inset shows the region around three-photon resonance ($\Delta_1 = 2\pi \times 4$ MHz). Other parameters are provided in text.

Figure 3.4 shows real part of probe coherence with respect to probe detuning, for changing n , with $r = 5 \mu m$. Starting with the non-interacting case, $n = 50, 60, 70, 80$ cases are displayed. Inset shows the region around three-photon resonance for clarity. As the interaction gets stronger blockade radius increases as well. When the atoms are inside blockaded region excitation to Rydberg state cannot be accomplished. Therefore as n increases, dispersive feature introduced by the EIT mechanism loses its effect.

Figure 3.5 shows the real part of probe coherence with respect to probe field detuning, for changing r with $n = 60$. Cases of $r = 1, 2, 4, 6 \mu m$ with $n = 60$ are shown. Inset shows the region around three-photon resonance for clarity. As in Figure 3.3, increasing interaction by means of closer atomic separation disrupt the EIT mechanism and steep dispersion curve introduced with EIT. In the case of $r = 1 \mu m$, dispersive property

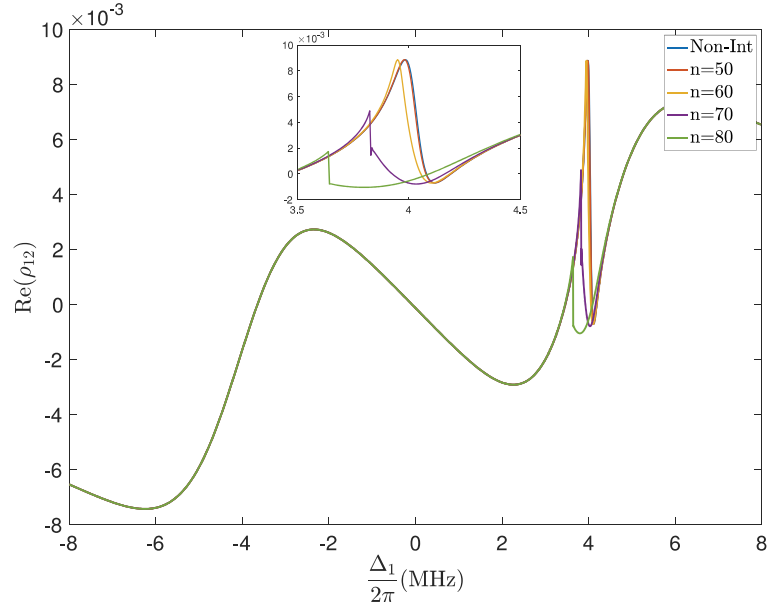


Figure 3.4. Real part of probe coherence with $r = 5 \mu m$ at different n , with respect to probe field detuning. Inset shows the region around three-photon resonance ($\Delta_1 = 2\pi \times 4$ MHz). Other parameters are provided in text.

occurring at three-photon resonance is lost.

As the atoms get closer to one another, van der Waals interaction increases further and at $r = 1 \mu m$ EIT is completely lost, meaning excitation to Rydberg state could not be achieved, making the system an effective three-level case. This is the limit of extreme interaction and in Figure 3.6 imaginary part and real part of probe coherence for a three-level case compared with a four-level case with inter-atomic distance being $r = 1 \mu m$ is shown.

In Figure 3.7 ground state populations with changing probe field detuning are shown for two cases; on the left side for different inter-atomic distances $r = 1, 2, 4, 6 \mu m$ with $n = 60$ and on the right side for different principal quantum numbers $n = 50, 60, 70, 80$ including non-interacting scenario with inter-atomic distance $r = 5 \mu m$. Insets show the region around three-photon resonance. In both cases, ground state population is at its lowest value when the three-photon resonance is achieved $\Delta_1 = 2\pi \times 4$ MHz. As the interaction increases by either increasing n or decreasing r , atoms are less likely to leave ground state. In the left side, at $n = 60$ blockade radius is $r_b = 5.31 \mu m$, therefore van

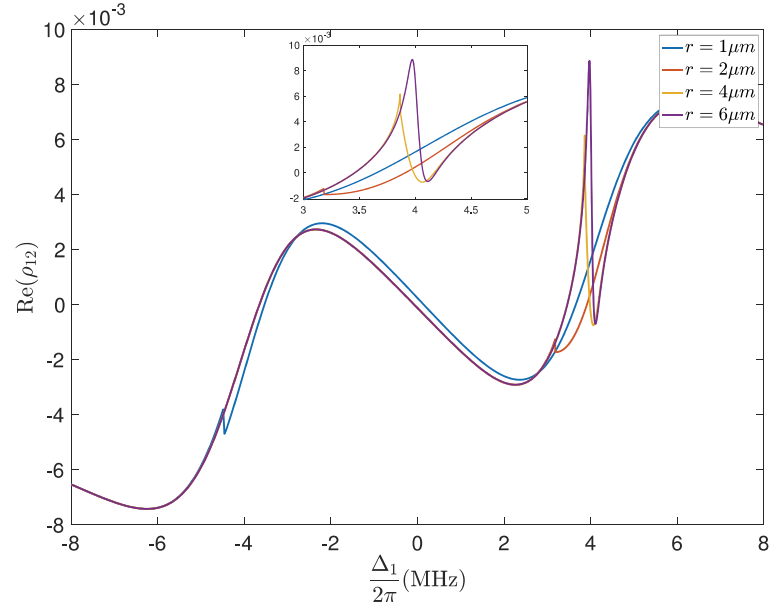


Figure 3.5. Real part of probe coherence at $n = 60$, with different r , with respect to probe field detuning. Inset shows the region around three-photon resonance ($\Delta_1 = 2\pi \times 4$ MHz). Other parameters are provided in text.

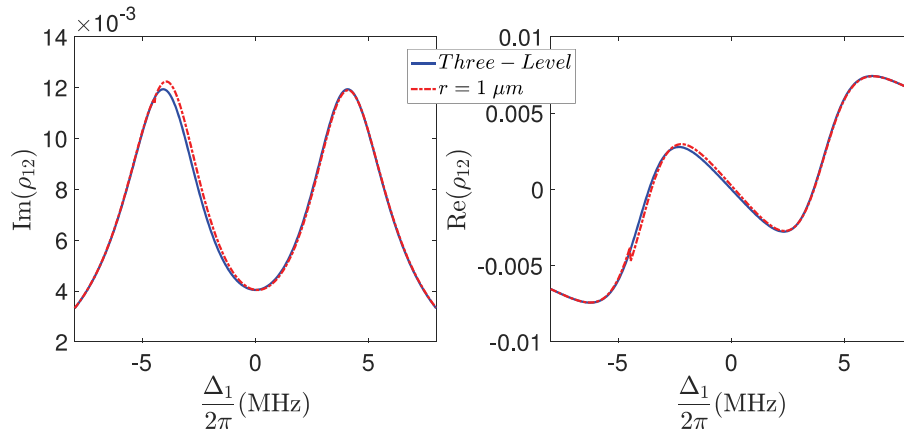


Figure 3.6. Imaginary part and real part of probe coherence with respect to probe field detuning for $r = 1 \mu m$ in the four-level case and a three-level case. **(Left)**, shows imaginary part of probe coherence and **(Right)** shows real part of probe coherence with different probe detunings. Other parameters are provided in text.

der Waals interaction becomes prominent when the atoms are placed closer than r_b . On the right side atomic separation is constant $r = 5 \mu m$ and at $n = 50$ blockade radius is $r_b = 3.66 \mu m$, so interaction effects can not be seen since atoms are well outside the blockade region.

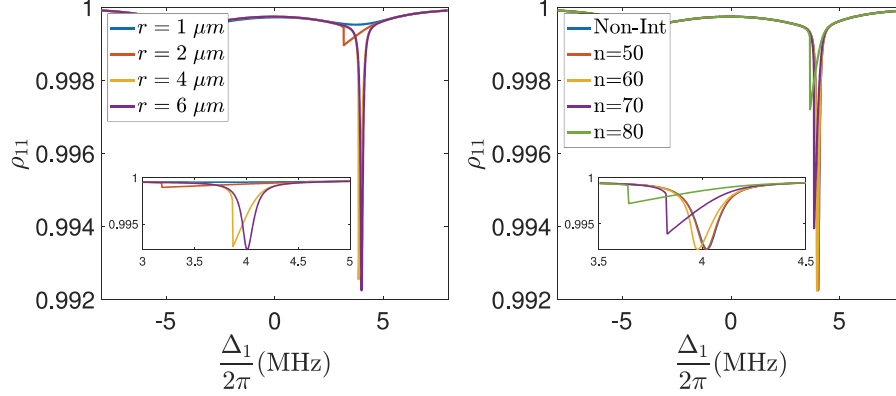


Figure 3.7. Ground state populations, with respect to probe field detuning for two cases: **(Left)** for different inter-atomic distances $r = 1, 2, 4, 6 \mu m$ with $n = 60$, **(Right)** for different principal quantum numbers $n = 50, 60, 70, 80$ including non-interacting scenario with inter-atomic distance $r = 5 \mu m$. Insets show the region around three-photon resonance ($\Delta_1 = 2\pi \times 4$ MHz). Other parameters are provided in text.

In Figure 3.8 Rydberg state populations with changing probe field detuning are shown for two cases; on the left side for different inter-atomic distances $r = 1, 2, 4, 6 \mu m$ with $n = 60$ and on the right side for different principal quantum numbers $n = 50, 60, 70, 80$ including non-interacting scenario with inter-atomic distance $r = 5 \mu m$. Insets show the region around three-photon resonance. In both cases, Rydberg state population is at its highest value at three-photon resonance $\Delta_1 = 2\pi \times 4$ MHz. As the interaction increases by either increasing n or decreasing r , atoms are less likely to be excited to Rydberg state. In the left side, at $n = 60$ blockade radius is $r_b = 5.31 \mu m$, therefore van der Waals interaction becomes prominent and excitation to Rydberg state decreases, when the atoms are placed closer than r_b . On the right side atomic separation is constant $r = 5 \mu m$ and at $n = 50$ blockade radius is $r_b = 3.66 \mu m$, so interaction effects can not be seen since atoms are well outside the blockade region.

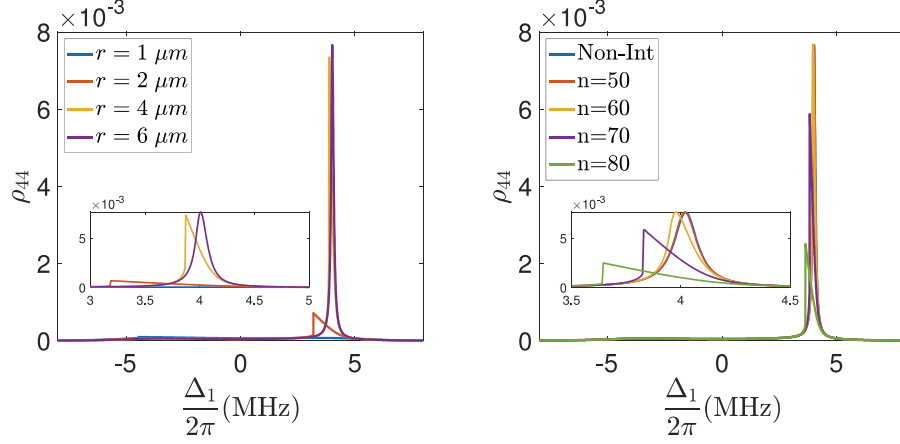


Figure 3.8. Rydberg state populations, with respect to probe field detuning for two cases: **(Left)** for different inter-atomic distances $r = 1, 2, 4, 6 \mu m$ with $n = 60$, **(Right)** for different principal quantum numbers $n = 50, 60, 70, 80$ including non-interacting scenario with inter-atomic distance $r = 5 \mu m$. Insets show the region around three-photon resonance ($\Delta_1 = 2\pi \times 4 \text{ MHz}$). Other parameters are provided in text.

3.1.2. Self-Consistent Mean-Field Algorithm

After considering two interacting Cs atoms case, we extended mean-field method to a self-consistent mean-field method in order to increase accuracy of the solutions for larger systems. Recalling many-body equations of motion within mean-field approximation in Eqn. 3.2, van der Waals interactions were in the form: $i \sum_{i \neq j} V_{ij} \rho_{\alpha 4}^{(i)} \rho_{44}^{(j)}$. It can be seen that; Rydberg state population ρ_{44} is common for every interaction term. Therefore we can write the van der Waals interaction for i^{th} atom as:

$$i \sum_{i \neq j} V_{ij} \rho_{\alpha 4}^{(i)} \rho_{44}^{(j)} = i \rho_{\alpha 4}^{(i)} \delta^{(j)}, \quad (3.4)$$

with, $\delta^{(i)} = \sum_{i \neq j} \frac{C_6}{|r_i - r_j|^6} \rho_{44}^{(j)}$. Our self-consistent mean-field approach starts with a random guess for average Rydberg state population ρ_{44} . Then, we distribute atoms randomly and calculate the sum of pairwise interactions for each atom based on the distance between each pair. After the interactions are added to the system, linearly coupled equa-

tions are solved for steady state Rydberg state population. Then the absolute difference between initial guess and solution for ρ_{44} is checked. If the difference is higher than a tolerance value, the solution for ρ_{44} is used as the new guess for the system. New steady state solution for ρ_{44} is acquired once again but with the previous solution as the initial guess for the system, then the difference between previous solution and new solution is checked, if the difference is larger than tolerance, same replacement takes place again. We expect this system to converge, therefore this replacement dynamic goes on until a difference smaller than tolerance is obtained. For the calculations statistical average is taken over 1000 realizations. Figure 3.9 shows the flowchart for self-consistent mean-field algorithm. MATLAB script used in production of figures in this Section is provided in Section A.2.

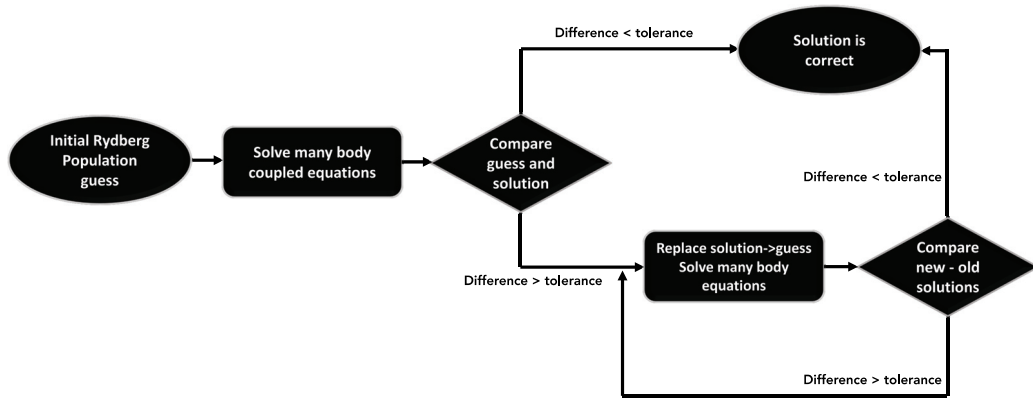


Figure 3.9. Self-consistent mean-field algorithm flowchart.

Calculations in this section consist of; imaginary part and real part of probe coherence, ground state and Rydberg state populations for steady state, for 50 atoms with respect to probe field detuning. Different cases of interactions, starting from the non-interacting case as a reference, $n = 50, 60, 70, 80, 90, 100$ are shown, data are statistically averaged over 1000 realizations. Insets in the following figures show the region zoomed around three-photon resonance $\Delta_1 = 2\pi \times 4$ MHz, for clarity. As the interaction increases, Rydberg blockade radius gets larger and more atoms are left inside blockaded region, therefore reducing the number of atoms in a Rydberg state at the same time. This

excitation suppression, traps atoms in the ground state, crippling the dark state formation, thus EIT and dispersive feature lose their prominence. Parameters used are the same as two-body system in Section 3.1.1.

Figure 3.10 shows the occurrence of induced transparency due to the strong dressing around three-photon resonance. Two absorption peaks at $\Delta_1 = 2\pi \times 4$ MHz and $\Delta_1 = -2\pi \times 4$ correspond to the absorption of the dressed states. But due to the dark state formation at three-photon resonance, absorption minima is observed instead of a peak.

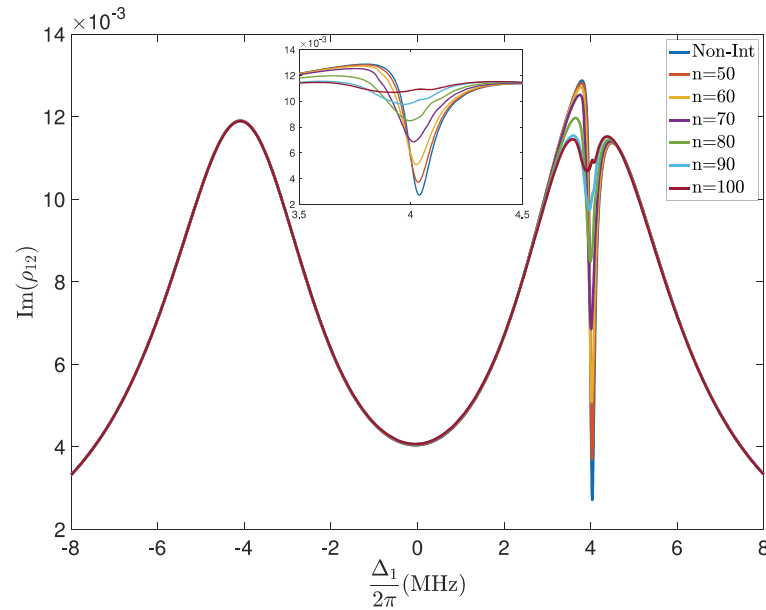


Figure 3.10. Imaginary part of probe coherence with respect to probe field detuning, with non-interacting case and $n = 50, 60, 70, 80, 90, 100$. Inset shows the zoomed in region around three-photon resonance $\Delta_1 = 2\pi \times 4$ MHz. Other parameters are provided in text.

Figure 3.11 shows the dispersive feature introduced by EIT mechanism at three-photon resonance. In the non-interacting case steep dispersion curve is observed, but as the van der Waals interaction gets stronger, slope of the dispersion curve gets smoother and at $n = 100$ as can be seen from the inset, steep curvature is completely lost.

Figures 3.12 shows the ground state populations for different interaction energies scanned across probe field detuning. Inset shows the region zoomed around three-photon

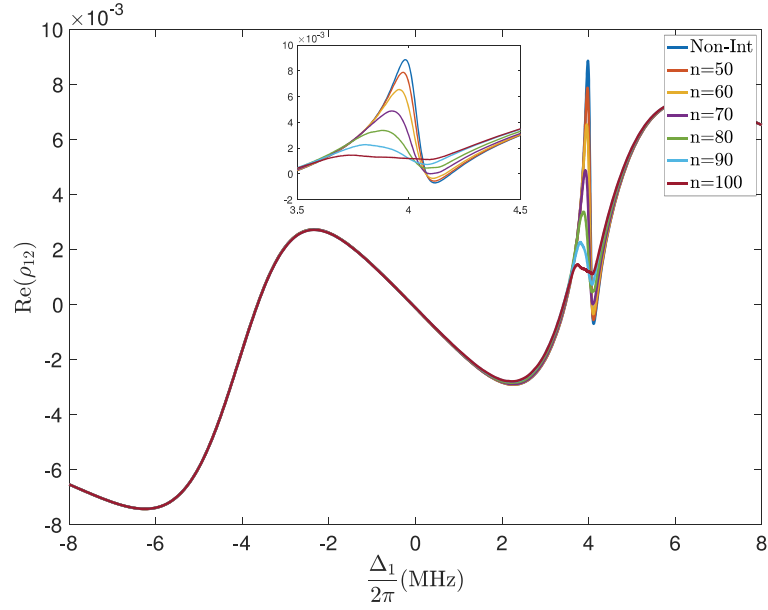


Figure 3.11. Real part of probe coherence with respect to probe field detuning, with non-interacting case and $n = 50, 60, 70, 80, 90, 100$. Inset shows the zoomed in region around three-photon resonance $\Delta_1 = 2\pi \times 4$ MHz. Other parameters are provided in text.

resonance $\Delta_1 = 2\pi \times 4$ MHz. Since the probe field is weak most of the population in the system is at ground state. At three-photon resonance, ground state population has the lowest value because excitation to Rydberg state is most effectively achieved at three-photon resonance. But as n increases, probability of exciting atoms from the ground state decreases, effectively trapping atoms at ground state.

Figure 3.13 shows the Rydberg state population with respect to probe field detuning for different interaction energies by means of changing principal quantum number n . Inset shows the region zoomed around three-photon resonance $\Delta_1 = 2\pi \times 4$ MHz. Highest Rydberg state population is achieved at three-photon resonance for every case of interaction including the non-interacting case. As the van der Waals interaction increases, Rydberg state population decreases. This happens because of the Rydberg blockade effect. As the interaction increases, number of atoms inside blockaded region increases, therefore reducing the number of Rydberg atoms inside the blockaded region.

Following calculations consist of; imaginary part and real part of probe coherence,

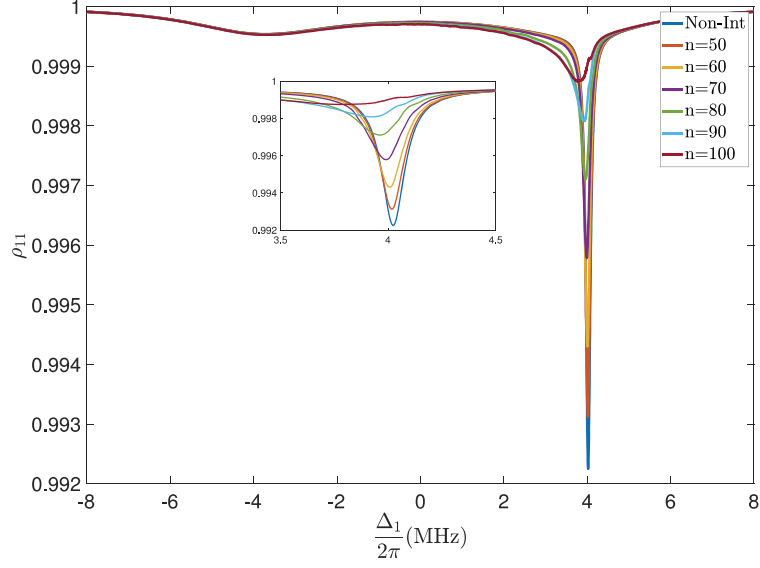


Figure 3.12. Ground state population with respect to probe field detuning, with non-interacting case and $n = 50, 60, 70, 80, 90, 100$. Inset shows the zoomed in region of three-photon resonance $\Delta_1 = 2\pi \times 4$ MHz. Other parameters are provided in text.

ground state and Rydberg state populations for steady state, for 50 atoms with respect to probe field detuning. van der Waals interaction is kept constant with $n = 60$, but different cases of dressing field detunings $\Delta_2 = 2\pi \times (-2, 0, 2, 4)$ MHz are shown, $\Delta_2 = 2\pi \times 0$ case is the reference case, since it is previously shown. Data are statistically averaged over 1000 realizations. Parameters used in the following figures (in MHz): $n = 60$, $\Omega_1 = 2\pi \times 0.1$, $\Omega_2 = 2\pi \times 8$, $\Omega_3 = 2\pi \times 1$, $\Gamma_1 = 2\pi \times 5.39$, $\Gamma_2 = 2\pi \times 1$, $\Gamma_3 = 0$, $\Delta_3 = -2\pi \times 4$. As the dressing field becomes off-resonant, EIT effect and dispersive feature shift toward three-photon resonance $\Delta_1 + \Delta_2 + \Delta_3 = 0$, meaning that three-photon resonance is required for formation of dark-state and energy crossings. And as the dressing field detuning changes, ground state population minimum and Rydberg state population maximum shifts toward three-photon resonance as well, implying that effective excitation from ground state is achieved at three-photon resonance.

Figure 3.14 shows imaginary part of probe coherence for different dressing field detunings with respect to probe field detuning. We expected to observe EIT behavior at three-photon resonance $\Delta_1 + \Delta_2 + \Delta_3 = 0$ and it can be seen that with changing Δ_2 EIT

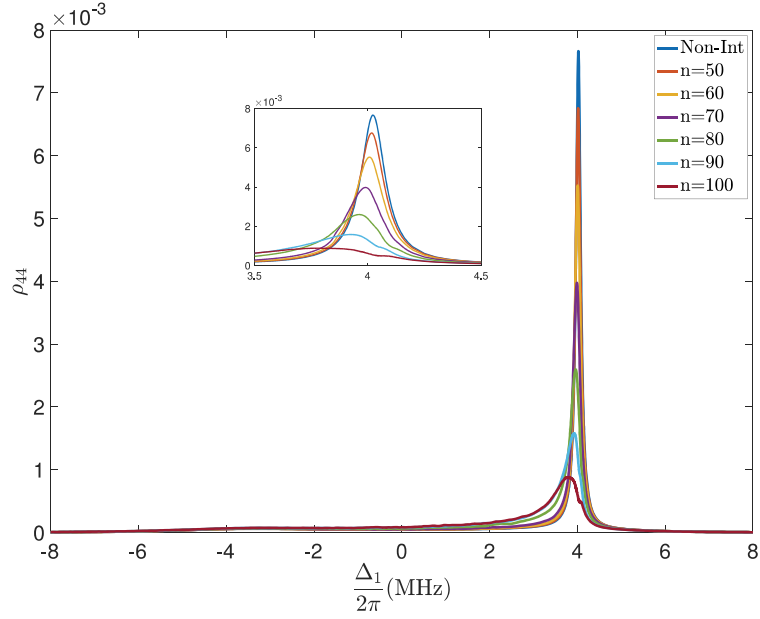


Figure 3.13. Rydberg state population with respect to probe field detuning, with non-interacting case and $n = 50, 60, 70, 80, 90, 100$. Inset shows the zoomed in region of three-photon resonance $\Delta_1 = 2\pi \times 4$ MHz. Other parameters are provided in text.

shifts towards three-photon resonance.

Figure 3.15 shows real part of probe coherence for different dressing field detunings with respect to probe field detuning. We expected to observe steep dispersion introduced by EIT mechanism at three-photon resonance $\Delta_1 + \Delta_2 + \Delta_3 = 0$ and steep change in refractive index shifts towards three-photon resonance with changing Δ_2 .

Figure 3.16 shows ground state population for different dressing field detunings with respect to probe field detuning. Excitation from ground state is most efficiently achieved at three-photon resonance meaning that ground state population has its lowest value at three-photon resonance. The case where $\Delta_2 = 2\pi \times 4$ MHz, is the lowest ground state population compared to other three cases. This is because in that case, probe field is on resonance with the transition from ground state to first excited state. And as the probe field detuning increases excitation from ground state decreases.

Figure 3.17 shows Rydberg state population for different dressing field detunings with respect to probe field detuning. Explanation for Figure 3.16 is also valid here. Since

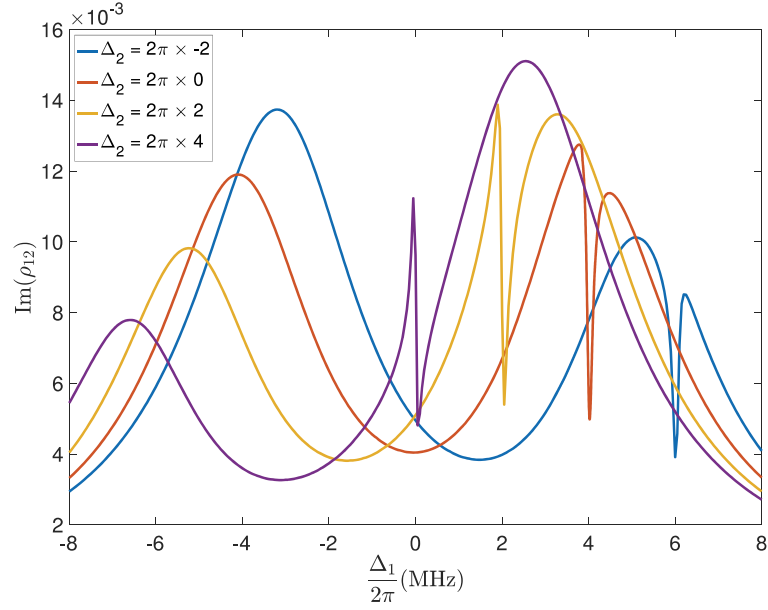


Figure 3.14. Imaginary part of probe coherence with respect to probe field detuning, with different dressing detunings $\Delta_2 = 2\pi \times (-2, 0, 2, 4)$. Other parameters are provided in text.

the excitation from ground state is most efficiently achieved with probe field on resonance, Rydberg state population has its highest value when the probe field is resonant with the transition.

We have seen that, a strong dressing field Ω_2 and a weak probe field Ω_1 in ladder configuration resulted in energy crossings and a dark-state to be formed. Dark-state formation at three-photon resonance ($\Delta_1 + \Delta_2 + \Delta_3 = 0$) allowed for a transparency window to be opened and with the inclusion of atomic interactions showed that EIT is prone to be disturbed. We observed that, van der Waals interactions affect the Rydberg population negatively. Calculations with changing dressing field detuning Δ_2 showed us that EIT effects are only seen at three-photon resonance.

In the next chapter, Rate Equation model will be explained and applied for the same Rydberg EIT configuration. Rate Equation model is another approach for studying many-body systems and it allows for a more accurate description and analysis of interacting many-body systems. In the Rate Equation model, we truncate the many-body dynamics to only include the state population rates.

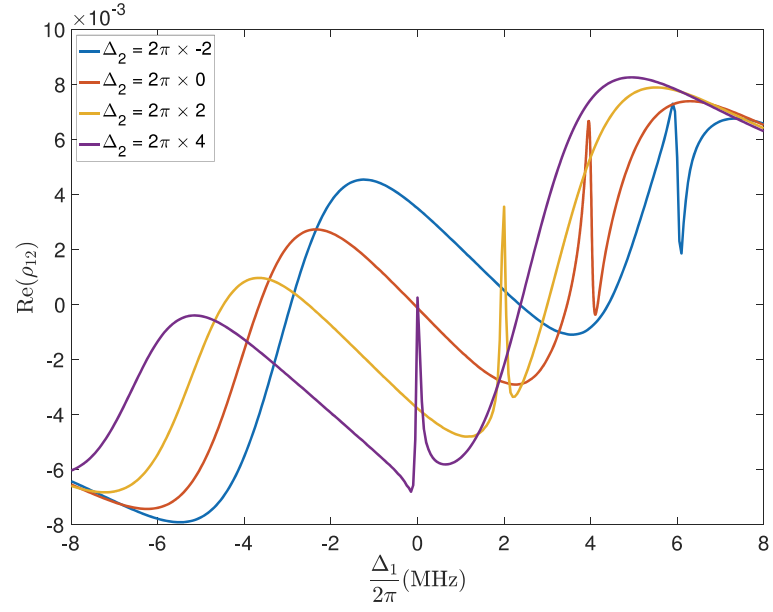


Figure 3.15. Real part of probe coherence with respect to probe field detuning, with different dressing detunings $\Delta_2 = 2\pi \times (-2, 0, 2, 4)$. Other parameters are provided in text.

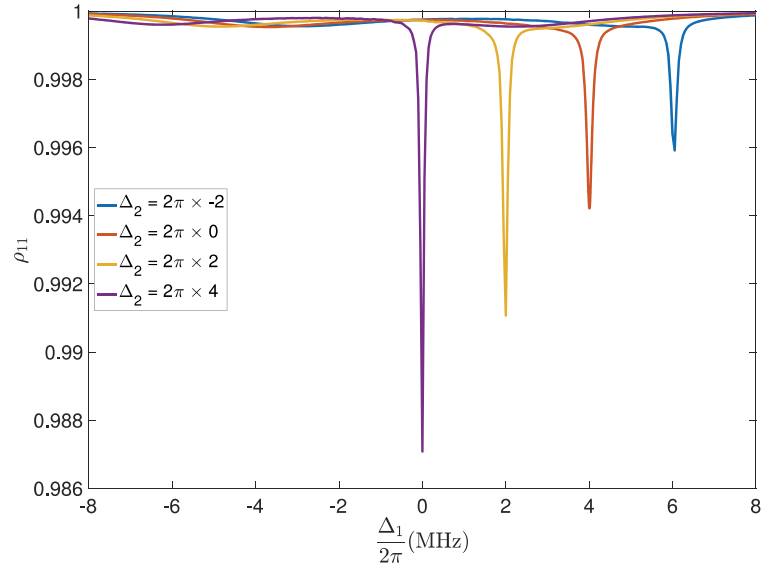


Figure 3.16. Ground state population with respect to probe field detuning, with different dressing detunings $\Delta_2 = 2\pi \times (-2, 0, 2, 4)$. Other parameters are provided in text.

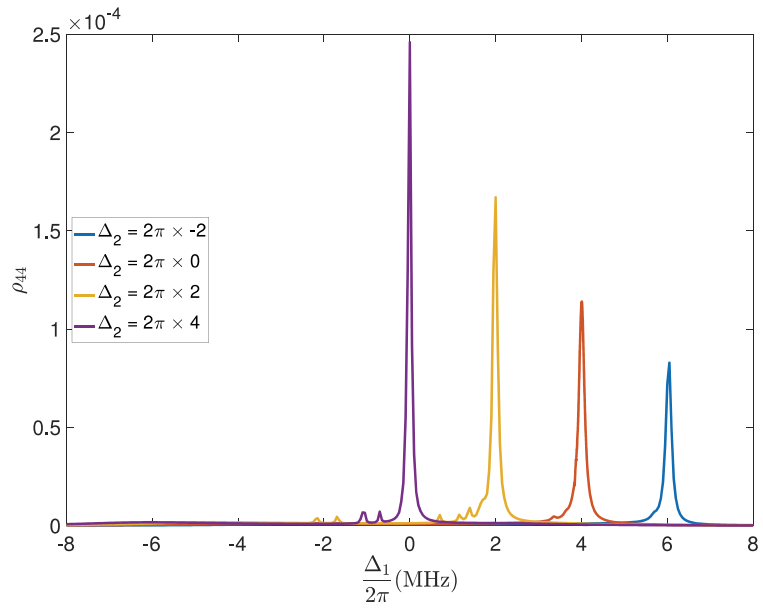


Figure 3.17. Rydberg state population with respect to probe field detuning, with different dressing detunings $\Delta_2 = 2\pi \times (-2, 0, 2, 4)$. Other parameters are provided in text.

CHAPTER 4

RATE EQUATION MODEL

After developing a self-consistent mean-field method, in order to achieve more accuracy we applied rate equation model to many-body system. Rate equation model, reduces the many-body dynamics to include only the population rates. Rate equation model is used in three-level Rydberg EIT schemes (Ates et al., 2006, 2007, 2011; Sevinçli et al., 2011). Methodology for the model is followed directly from the literature. Firstly, we assume that there is no interaction present in the system $V_{ij} = 0$. Then many-body equations of motion in Eqn. (2.22) reduces to single particle OBEs in Eqn. (2.20). Following that we assume, coherences $\rho_{\alpha\beta}$, $\alpha \neq \beta$ evolve slowly compared to the populations $\rho_{\alpha\alpha}$. This enables us to adiabatically eliminate coherences $\dot{\rho}_{\alpha\beta} = 0$. After that we performed a linear solution over coherences and we acquired rate equations for populations for a single-body:

$$\frac{d}{dt} \begin{pmatrix} \rho_{11} \\ \rho_{22} \\ \rho_{33} \\ \rho_{44} \end{pmatrix} = \begin{pmatrix} -a_{11} & a_{12} & a_{13} & a_{14} \\ a_{21} & -a_{22} & a_{23} & a_{24} \\ a_{31} & a_{32} & -a_{33} & a_{34} \\ a_{41} & a_{42} & a_{43} & -a_{44} \end{pmatrix} \begin{pmatrix} \rho_{11} \\ \rho_{22} \\ \rho_{33} \\ \rho_{44} \end{pmatrix}. \quad (4.1)$$

Here, coefficient matrix of populations are called the bare transition rate matrix and $a_{\alpha\beta}$ are transition rates. But some of the transition rates might be negative which is not physical (Wilcox and Lamb, 1960). To overcome this issue we perform a linear transformation to remove the negative rates while preserving the same steady state solutions. Then, following along the literature, we introduce the following correction matrix as:

$$\Delta a = \begin{pmatrix} \sigma_{21} + \sigma_{31} + \sigma_{41} & -k_3 + \sigma_{21} + \sigma_{23} + \sigma_{24} + \sigma_{32} + \sigma_{42} & -k_2 + \sigma_{23} + \sigma_{31} + \sigma_{32} + \sigma_{34} + \sigma_{43} & -k_1 + \sigma_{24} + \sigma_{34} + \sigma_{41} + \sigma_{42} + \sigma_{43} \\ -\sigma_{21} & k_3 - \sigma_{21} - \sigma_{23} - \sigma_{24} & -\sigma_{23} & -\sigma_{24} \\ -\sigma_{31} & -\sigma_{32} & k_2 - \sigma_{31} - \sigma_{32} - \sigma_{34} & -\sigma_{34} \\ -\sigma_{41} & -\sigma_{42} & -\sigma_{43} & k_1 - \sigma_{41} - \sigma_{42} - \sigma_{43} \end{pmatrix},$$

with $\sigma_{\alpha\beta} = \frac{a_{\alpha\beta} - |a_{\alpha\beta}|}{2}$ and k_1, k_2, k_3 are constants chosen so $\dot{\rho} = (a + \Delta a)\rho$ will yield the same steady states as: $\dot{\rho} = a\rho$. After obtaining the correct transformed rates, we introduce the interaction as a local detuning, since we only consider Rydberg

state interactions, in order to extend the single-body system to include many-body effects. Local detuning is defined as follows:

$$\Delta_3^{(i)} = \Delta_3 - \sum_{i \neq j} \frac{C_6}{|r_i - r_j|^6} . \quad (4.2)$$

Here, summation term is over Rydberg atoms only. Then in order to acquire steady state populations we used Monte-Carlo sampling. Monte-Carlo sampling is especially useful when acquiring a deterministic result to a probabilistic problem. In our Monte-Carlo algorithm: atoms are randomly distributed and initialized in ground state. Then, random transitions are performed according to transition probabilities determined by transition rates. Probability of transition between state α and state β is defined as:

$$P_{\alpha \rightarrow \beta}^{(i)} = \delta_t (a + \Delta a)_{\alpha\beta} . \quad (4.3)$$

Here $P_{\alpha \rightarrow \beta}^{(i)}$ is the probability of transition between state α and state β , δ_t is the time step, which is defined as; every increment of transition. Total time is determined by the time it takes for the populations to reach a steady state. Then, we roll a die for every time step for every atom and compare the probability of the atom leaving its current state with die. If the die is smaller than the probability, transition occurs. Since we are only interested in the interactions caused by Rydberg atoms, when an atom transitions to Rydberg state, we calculate Rydberg interaction with every other atom and add the interaction energy to that atom's Rydberg state detuning value as in Eqn. (4.2). Therefore when the Rydberg state detuning changes, the probability of exciting that atom to a Rydberg state changes as well. Figure 4.1 shows a flowchart for the Monte-Carlo sampling. MATLAB script for Monte-Carlo algorithm is provided in Section A.3.

Since our system at hand is a four-level scheme, we have 16 coefficients that govern populations and transitions. And even for a small system of 100 atoms, performing a statistically averaged Monte-Carlo sampling over 100 realizations is extremely time consuming. Unfortunately due to lack of time and computational power we could not perform this calculation in the time frame of this thesis. A possible solution to this issue is using the effective operator formalism method (Reiter and Sørensen, 2012). In this method, effective operators are defined for the system in order to reduce the evolution of system



Figure 4.1. Rate equation model Monte-Carlo algorithm flowchart.

dynamics. It would be possible to reduce the four-level system into an effective three-level system. There are several applications of effective operator formalism on literature and it is observed to be in good agreement with the experimental results (Reiter et al., 2012; Schempp et al., 2015). It is also reportedly possible to apply rate equation model with atom pair treatment (Heeg et al., 2012). This hybrid model too, has potential to reduce the complexity of our problem.

CHAPTER 5

CONCLUSION

In this thesis, Electromagnetically Induced Transparency in a four-level Rydberg scheme is analyzed and effect of Rydberg-Rydberg interactions on EIT behavior is studied. In the Introduction Chapter, EIT scheme in a three-level lambda system with strong coupling field and weak probe field, is explained by dressed-state formalism. First Hamiltonian for a three-level lambda system is derived within dipole and rotating wave approximations. Then dressed states are acquired and the formation of a dark-state with zero eigenvalue was shown. Moreover, absence of absorption for the probe field is explained by the dark-state. Following that; optical response in terms of absorption and refractive index for an atomic medium is explained. Rydberg blockade mechanism due to van der Waals interaction is discussed.

Afterwards, in Theory Chapter; atom-light interaction terms for a four-level ladder system is obtained and Optical Bloch Equations are acquired. Followed by discussions of steady state solutions and avoided crossings corresponding to absorptive features. Later, many-body equations of motion for interacting system are derived. Many-body equations are not solvable due to the hierarchy introduced by two-body density matrices, therefore two approaches to tackle this problem is employed. In the first approach, mean-field approximation is used to reduce two-body density matrices into product of single-body density matrices. First interacting two-body case is analyzed in detail. Optical response of the medium and ground state and Rydberg state populations are studied in detail for different interaction energies. Rydberg blockade effect on optical properties and state populations are discussed. After that, in order to study larger systems with more accuracy, self-consistent mean-field method is developed. Effects of Rydberg interaction and Rydberg blockade on optical properties as well as state populations are analyzed. In the second approach, rate equation method is adopted. After adiabatic elimination of coherences, rate equations for populations are obtained and a Monte-Carlo algorithm is developed in order to solve the system. Due to inadequacies in time and computation power, rate equation method could not be completed within the time frame of this thesis.

A possible remedy to this problem is to reduce the four-level system into an effective three-level system. This can be achieved by effective operator formalism method and will be pursued in the future.

In conclusion; EIT phenomenon is extended to a four-level ladder scheme in which fourth level is a Rydberg state. Presence of transparency due to dark-state formation is analyzed in detail. Effects of Rydberg-Rydberg interactions on EIT features are studied. It is observed that; as the van der Waals interaction increases either by means of increasing principal quantum number or by decreasing inter-atomic distance, Rydberg blockade becomes more effective and transparency weakens. In the limit of extreme interaction, excitation to Rydberg state could not be achieved and four-level system transforms to an effective three-level system without the Rydberg state and transparency is completely lost.

REFERENCES

- Abi-Salloum, T. Y. (2010, May). Electromagnetically induced transparency and autler-townes splitting: Two similar but distinct phenomena in two categories of three-level atomic systems. *Phys. Rev. A* 81, 053836.
- Afrousheh, K., P. Bohlouli-Zanjani, D. Vagale, A. Mugford, M. Fedorov, and J. D. D. Martin (2004, Nov). Spectroscopic observation of resonant electric dipole-dipole interactions between cold rydberg atoms. *Phys. Rev. Lett.* 93, 233001.
- Allen, L. and J. H Eberly (1987, Jan). *Optical Resonance and Two-Level Atoms*.
- Ates, C., T. Pohl, T. Pattard, and J. M. Rost (2006, May). Strong interaction effects on the atom counting statistics of ultracold rydberg gases. *Journal of Physics B: Atomic, Molecular and Optical Physics* 39(11), L233–L239.
- Ates, C., T. Pohl, T. Pattard, and J. M. Rost (2007, Jul). Many-body theory of excitation dynamics in an ultracold rydberg gas. *Phys. Rev. A* 76, 013413.
- Ates, C., S. Sevinçli, and T. Pohl (2011, Apr). Electromagnetically induced transparency in strongly interacting rydberg gases. *Phys. Rev. A* 83, 041802.
- Autler, S. H. and C. H. Townes (1955, Oct). Stark effect in rapidly varying fields. *Phys. Rev.* 100, 703–722.
- Barnett, S. and P. Radmore (2002). *Methods in Theoretical Quantum Optics*. Oxford: Oxford University Press.
- Bason, M. G., A. K. Mohapatra, K. J. Weatherill, and C. S. Adams (2008, Mar). Electro-optic control of atom-light interactions using rydberg dark-state polaritons. *Phys. Rev. A* 77, 032305.
- Bhushan, S., V. S. Chauhan, and R. K. Easwaran (2018). Ultracold rydberg atoms for

efficient storage of terahertz frequency signals using electromagnetically induced transparency. *Physics Letters A* 382(48), 3500 – 3504.

Bloch, F. (1946, Oct). Nuclear induction. *Phys. Rev.* 70, 460–474.

Boller, K.-J., A. Imamoglu, and S. E. Harris (1991, May). Observation of electromagnetically induced transparency. *Phys. Rev. Lett.* 66, 2593–2596.

Boyd, R. W. (2008). *Nonlinear Optics, Third Edition* (3rd ed.). Orlando, FL, USA: Academic Press, Inc.

Budker, D., D. F. Kimball, S. M. Rochester, and V. V. Yashchuk (1999, Aug). Nonlinear magneto-optics and reduced group velocity of light in atomic vapor with slow ground state relaxation. *Phys. Rev. Lett.* 83, 1767–1770.

Carr, C., M. Tanasittikosol, A. Sargsyan, D. Sarkisyan, C. S. Adams, and K. J. Weatherill (2012, Sep). Three-photon electromagnetically induced transparency using rydberg states. *Opt. Lett.* 37(18), 3858–3860.

Chanelière, T., D. N. Matsukevich, S. D. Jenkins, S.-Y. Lan, T. A. B. Kennedy, and A. Kuzmich (2005). Storage and retrieval of single photons transmitted between remote quantum memories. *Nature* 438(7069), 833–836.

Chotia, A., M. Viteau, T. Vogt, D. Comparat, and P. Pillet (2008, apr). Kinetic monte carlo modeling of dipole blockade in rydberg excitation experiment. *New Journal of Physics* 10(4), 045031.

Cohen-Tannoudji, C. (1998). Manipulating atoms with photons. *Physica Scripta* T76(1), 33.

Eisaman, M. D., A. André, F. Massou, M. Fleischhauer, A. S. Zibrov, and M. D. Lukin (2005). Electromagnetically induced transparency with tunable single-photon pulses. *Nature* 438(7069), 837–841.

Firstenberg, O., C. S. Adams, and S. Hofferberth (2016, jun). Nonlinear quantum optics mediated by rydberg interactions. *Journal of Physics B: Atomic, Molecular and Optical Physics* 49(15), 152003.

Fleischhauer, M., C. H. Keitel, M. O. Scully, C. Su, B. T. Ulrich, and S.-Y. Zhu (1992, Aug). Resonantly enhanced refractive index without absorption via atomic coherence. *Phys. Rev. A* 46, 1468–1487.

Fleischhauer, M. and M. D. Lukin (2000, May). Dark-state polaritons in electromagnetically induced transparency. *Phys. Rev. Lett.* 84, 5094–5097.

Friedler, I., D. Petrosyan, M. Fleischhauer, and G. Kurizki (2005, Oct). Long-range interactions and entanglement of slow single-photon pulses. *Phys. Rev. A* 72, 043803.

Gaëtan, A., Y. Miroshnychenko, T. Wilk, A. Chotia, M. Viteau, D. Comparat, P. Pillet, A. Browaeys, and P. Grangier (2009, Jan). Observation of collective excitation of two individual atoms in the rydberg blockade regime. *Nature Physics* 5, 115 EP –.

Gallagher, T. F. (1994). *Rydberg Atoms*. Cambridge Monographs on Atomic, Molecular and Chemical Physics. Cambridge University Press.

Gavryusev, V., M. Ferreira-Cao, A. Kekic, G. Zürn, and A. Signoles (2016). Interaction enhanced imaging of rydberg p states. *The European Physical Journal Special Topics* 225(15), 2863–2889.

Gerry, C. and P. Knight (2004). *Introductory Quantum Optics*. Cambridge University Press.

Günter, G., M. Robert-de Saint-Vincent, H. Schempp, C. S. Hofmann, S. Whitlock, and M. Weidemüller (2012, Jan). Interaction enhanced imaging of individual rydberg atoms in dense gases. *Phys. Rev. Lett.* 108, 013002.

Günter, G., H. Schempp, M. Robert-de Saint-Vincent, V. Gavryusev, S. Helmrich, C. S. Hofmann, S. Whitlock, and M. Weidemüller (2013). Observing the dynamics of

dipole-mediated energy transport by interaction-enhanced imaging. *Science* 342(6161), 954–956.

Hakuta, K., L. Marmet, and B. P. Stoicheff (1991, Feb). Electric-field-induced second-harmonic generation with reduced absorption in atomic hydrogen. *Phys. Rev. Lett.* 66, 596–599.

Harris, S. E., J. E. Field, and A. Imamoglu (1990, Mar). Nonlinear optical processes using electromagnetically induced transparency. *Phys. Rev. Lett.* 64, 1107–1110.

Hau, L. V., S. E. Harris, Z. Dutton, and C. H. Behroozi (1999). Light speed reduction to 17 metres per second in an ultracold atomic gas. *Nature* 397(6720), 594–598.

Heeg, K. P., M. Gärttner, and J. Evers (2012, Dec). Hybrid model for rydberg gases including exact two-body correlations. *Phys. Rev. A* 86, 063421.

Heidemann, R., U. Raitzsch, V. Bendkowsky, B. Butscher, R. Löw, L. Santos, and T. Pfau (2007, Oct). Evidence for coherent collective rydberg excitation in the strong blockade regime. *Phys. Rev. Lett.* 99, 163601.

Šibalić, N., J. M. Kondo, C. S. Adams, and K. J. Weatherill (2016, Sep). Dressed-state electromagnetically induced transparency for light storage in uniform-phase spin waves. *Phys. Rev. A* 94, 033840.

Jackson, J. D. (1999). *Classical electrodynamics* (3rd ed. ed.). New York, NY: Wiley.

Kang, H. and Y. Zhu (2003, Aug). Observation of large kerr nonlinearity at low light intensities. *Phys. Rev. Lett.* 91, 093601.

Kash, M. M., V. A. Sautenkov, A. S. Zibrov, L. Hollberg, G. R. Welch, M. D. Lukin, Y. Rostovtsev, E. S. Fry, and M. O. Scully (1999, Jun). Ultraslow group velocity and enhanced nonlinear optical effects in a coherently driven hot atomic gas. *Phys. Rev. Lett.* 82, 5229–5232.

Lesanovsky, I., B. Olmos, and J. P. Garrahan (2010, Sep). Thermalization in a coherently driven ensemble of two-level systems. *Phys. Rev. Lett.* 105, 100603.

Liebisch, T. C., A. Reinhard, P. R. Berman, and G. Raithel (2005, Dec). Atom counting statistics in ensembles of interacting rydberg atoms. *Phys. Rev. Lett.* 95, 253002.

Liu, C., Z. Dutton, C. H. Behroozi, and L. V. Hau (2001). Observation of coherent optical information storage in an atomic medium using halted light pulses. *Nature* 409(6819), 490–493.

LL.D., J. K. (1875). XI. a new relation between electricity and light: Dielectrified media birefringent. *The London, Edinburgh, and Dublin Philosophical Magazine and Journal of Science* 50(332), 337–348.

Lukin, M. D. (2003, Apr). Colloquium: Trapping and manipulating photon states in atomic ensembles. *Rev. Mod. Phys.* 75, 457–472.

Lukin, M. D., M. Fleischhauer, R. Cote, L. M. Duan, D. Jaksch, J. I. Cirac, and P. Zoller (2001, Jun). Dipole blockade and quantum information processing in mesoscopic atomic ensembles. *Phys. Rev. Lett.* 87, 037901.

Mauger, S., J. Millen, and M. P. A. Jones (2007, nov). Spectroscopy of strontium rydberg states using electromagnetically induced transparency. *Journal of Physics B: Atomic, Molecular and Optical Physics* 40(22), F319–F325.

Mohapatra, A. K., M. G. Bason, B. Butscher, K. J. Weatherill, and C. S. Adams (2008, Sep). A giant electro-optic effect using polarizable dark states. *Nature Physics* 4, 890 EP –. Article.

Mohapatra, A. K., T. R. Jackson, and C. S. Adams (2007, Mar). Coherent optical detection of highly excited rydberg states using electromagnetically induced transparency. *Phys. Rev. Lett.* 98, 113003.

P. Abel, R., A. Mohapatra, M. Bason, J. D. Pritchard, K. Weatherill, U. Krohn, and

C. Adams (2009, 03). Laser frequency stabilization to excited state transitions using electromagnetically induced transparency in a cascade system. *Applied Physics Letters* 94, 071107 – 071107.

Phillips, D. F., A. Fleischhauer, A. Mair, R. L. Walsworth, and M. D. Lukin (2001, Jan). Storage of light in atomic vapor. *Phys. Rev. Lett.* 86, 783–786.

Reiter, F., M. J. Kastoryano, and A. S. Sørensen (2012). Driving two atoms in an optical cavity into an entangled steady state using engineered decay. *14*(5), 053022.

Reiter, F. and A. S. Sørensen (2012, Mar). Effective operator formalism for open quantum systems. *Phys. Rev. A* 85, 032111.

Schempp, H., G. Günter, C. S. Hofmann, C. Giese, S. D. Saliba, B. D. DePaola, T. Amthor, M. Weidemüller, S. Sevinçli, and T. Pohl (2010, Apr). Coherent population trapping with controlled interparticle interactions. *Phys. Rev. Lett.* 104, 173602.

Schempp, H., G. Günter, S. Wüster, M. Weidemüller, and S. Whitlock (2015, Aug). Correlated exciton transport in rydberg-dressed-atom spin chains. *Phys. Rev. Lett.* 115, 093002.

Schmidt, H. and A. Imamoglu (1996, Dec). Giant kerr nonlinearities obtained by electromagnetically induced transparency. *Opt. Lett.* 21(23), 1936–1938.

Sedlacek, J. A., A. Schwettmann, H. Kübler, R. Löw, T. Pfau, and J. P. Shaffer (2012, Sep). Microwave electrometry with rydberg atoms in a vapour cell using bright atomic resonances. *Nature Physics* 8, 819 EP –. Article.

Sevinçli, S., C. Ates, T. Pohl, H. Schempp, C. S. Hofmann, G. Günter, T. Amthor, M. Weidemüller, J. D. Pritchard, D. Maxwell, A. Gauguet, K. J. Weatherill, M. P. A. Jones, and C. S. Adams (2011, sep). Quantum interference in interacting three-level rydberg gases: coherent population trapping and electromagnetically induced transparency. *Journal of Physics B: Atomic, Molecular and Optical Physics* 44(18), 184018.

Simon, C., M. Afzelius, J. Appel, A. Boyer de la Giroday, S. J. Dewhurst, N. Gisin, C. Y. Hu, F. Jelezko, S. Kröll, J. H. Müller, J. Nunn, E. S. Polzik, J. G. Rarity, H. De Riedmatten, W. Rosenfeld, A. J. Shields, N. Sköld, R. M. Stevenson, R. Thew, I. A. Walmsley, M. C. Weber, H. Weinfurter, J. Wrachtrup, and R. J. Young (2010, May). Quantum memories. *The European Physical Journal D* 58(1), 1–22.

Singer, K., M. Reetz-Lamour, T. Amthor, L. G. Marcassa, and M. Weidemüller (2004, Oct). Suppression of excitation and spectral broadening induced by interactions in a cold gas of rydberg atoms. *Phys. Rev. Lett.* 93, 163001.

Singer, K., J. Stanojevic, M. Weidemüller, and R. Côté (2005, jan). Long-range interactions between alkali rydberg atom pairs correlated to their asymptotes. *Journal of Physics B: Atomic, Molecular and Optical Physics* 38(2), S295–S307.

Thoumany, P., T. Germann, T. Hänsch, G. Stania, L. Urbonas, and T. Becker (2009, Oct). Spectroscopy of rubidium rydberg states with three diode lasers. *Journal of Modern Optics* 56(18-19), 2055–2060.

Tong, D., S. M. Farooqi, J. Stanojevic, S. Krishnan, Y. P. Zhang, R. Côté, E. E. Eyler, and P. L. Gould (2004, Aug). Local blockade of rydberg excitation in an ultracold gas. *Phys. Rev. Lett.* 93, 063001.

Urban, E., T. A. Johnson, T. Henage, L. Isenhower, D. D. Yavuz, T. G. Walker, and M. Saffman (2009, Jan). Observation of rydberg blockade between two atoms. *Nature Physics* 5, 110 EP –.

van Ditzhuijzen, C. S. E., A. F. Koenderink, J. V. Hernández, F. Robicheaux, L. D. Noordam, and H. B. v. L. van den Heuvel (2008, Jun). Spatially resolved observation of dipole-dipole interaction between rydberg atoms. *Phys. Rev. Lett.* 100, 243201.

Vogt, T., M. Viteau, A. Chotia, J. Zhao, D. Comparat, and P. Pillet (2007, Aug). Electric-field induced dipole blockade with rydberg atoms. *Phys. Rev. Lett.* 99, 073002.

Vogt, T., M. Viteau, J. Zhao, A. Chotia, D. Comparat, and P. Pillet (2006, Aug). Dipole blockade at Förster resonances in high resolution laser excitation of Rydberg states of cesium atoms. *Phys. Rev. Lett.* *97*, 083003.

Wade, C. G., M. Marcuzzi, E. Levi, J. M. Kondo, I. Lesanovsky, C. S. Adams, and K. J. Weatherill (2018). A terahertz-driven non-equilibrium phase transition in a room temperature atomic vapour. *Nature Communications* *9*(1), 3567.

Weatherill, K. J., J. D. Pritchard, R. P. Abel, M. G. Bason, A. K. Mohapatra, and C. S. Adams (2008, Oct). Electromagnetically induced transparency of an interacting cold Rydberg ensemble. *Journal of Physics B: Atomic, Molecular and Optical Physics* *41*(20), 201002.

Weimer, H., R. Löw, T. Pfau, and H. P. Büchler (2008, Dec). Quantum critical behavior in strongly interacting Rydberg gases. *Phys. Rev. Lett.* *101*, 250601.

Wilcox, L. R. and W. E. Lamb (1960, Sep). Fine structure of short-lived states of hydrogen by a microwave-optical method. ii. *Phys. Rev.* *119*, 1915–1933.

APPENDIX A

MATLAB SCRIPTS

In Appendix, three MATLAB scripts are provided. In Section A.1, script for, steady state solutions of coherences and populations for Optical Bloch Equations is provided. In Section A.2, self-consistent mean-field algorithm is provided and in Section A.3 Monte-Carlo algorithm used for rate equation method is provided.

A.1. Steady State Solutions for OBEs

MATLAB script for calculating steady state solutions for coherences and populations from OBEs are presented. Figure 2.2 is obtained by using this code.

```
1 % This code, calculates the coherences and populations for a four-level
2 % ladder system in steady state.
3
4 % System parameters
5
6 % Rabi frequencies for probe, dressing and coupling fields:
7
8 w1 = 2*pi*(0.1);
9 w2 = 2*pi*(8);
10 w3 = 2*pi*(0.5);
11
12 % Field detunings:
13
14 det2 = 2*pi*(0);
15 det3 = 2*pi*(-4);
16
17 % Radiative decay rates:
18
19 g1 = 2*pi*(1);
20 g2 = 2*pi*(1);
21 g3 = 0;
22
23 % Probe detuning to be scanned:
24
25 prob_det = -2*pi*8:2*pi*0.001:2*pi*8;
26
27 i=1; % Dummy variable
```

```

28
29 % This loop solves the linearly coupled set of equations for every probe
30 % detuning.
31
32 for det1=-8:0.001:8
33     % d_rho = Coeffs * rho
34     % Coefficient matrix resulting from the Master Eqn.
35
36     Coeffs(:, :, i)=[ 0, (w1*1i)/2, 0, 0, -(w1*1i)/2, g1, 0, 0, 0, 0, 0, 0, 0, 0, 0,
37                       0;...
38                       (w1*1i)/2, -g1/2 - pi*det1*2i, (w2*1i)/2, 0, 0, -(w1*1i)/2, 0, 0, 0, 0, 0,
39                       0, 0, 0, 0, 0;...
40                       0, (w2*1i)/2, -det2*1i - g2/2 - pi*det1*2i, (w3*1i)/2, 0, 0, -(w1*1i)/2, 0,
41                       0, 0, 0, 0, 0, 0, 0;...
42                       0, 0, (w3*1i)/2, -det2*1i - det3*1i - pi*det1*2i, 0, 0, 0, -(w1*1i)/2, 0,
43                       0, 0, 0, 0, 0, 0, 0;...
44                       -(w1*1i)/2, 0, 0, 0, -g1/2 + pi*det1*2i, (w1*1i)/2, 0, 0, -(w2*1i)/2, 0, 0,
45                       0, 0, 0, 0, 0;...
46                       0, -(w1*1i)/2, 0, 0, (w1*1i)/2, -g1, (w2*1i)/2, 0, 0, -(w2*1i)/2, g2, 0, 0,
47                       0, 0, 0;...
48                       0, 0, -(w1*1i)/2, 0, 0, (w2*1i)/2, -det2*1i - g1/2 - g2/2, (w3*1i)/2, 0, 0,
49                       -(w2*1i)/2, 0, 0, 0, 0, 0;...
50                       0, 0, 0, -(w1*1i)/2, 0, 0, (w3*1i)/2, -det2*1i - det3*1i - g1/2, 0, 0, 0,
51                       -(w2*1i)/2, 0, 0, 0;...
52                       0, 0, 0, 0, -(w2*1i)/2, 0, 0, 0, det2*1i - g2/2 + pi*det1*2i, (w1*1i)/2, 0,
53                       0, -(w3*1i)/2, 0, 0, 0;...
54                       0, 0, 0, 0, 0, -(w2*1i)/2, 0, 0, (w1*1i)/2, det2*1i - g1/2 - g2/2, (w2*1i)
55                       /2, 0, 0, -(w3*1i)/2, 0, 0;...
56                       0, 0, 0, 0, 0, 0, -(w2*1i)/2, 0, 0, (w2*1i)/2, -g2, (w3*1i)/2, 0, 0, -(w3*1i)
57                       )/2, 0;...
58                       0, 0, 0, 0, 0, 0, 0, -(w2*1i)/2, 0, 0, (w3*1i)/2, -det3*1i - g2/2, 0, 0, 0,
59                       -(w3*1i)/2;...
60                       0, 0, 0, 0, 0, 0, 0, 0, 0, -(w3*1i)/2, 0, 0, 0, det2*1i + det3*1i + pi*det1*2i,
61                       (w1*1i)/2, 0, 0;...
62                       0, 0, 0, 0, 0, 0, 0, 0, 0, 0, -(w3*1i)/2, 0, 0, (w1*1i)/2, det2*1i + det3*1i -
63                       g1/2, (w2*1i)/2, 0;...
64                       0, 0, 0, 0, 0, 0, 0, 0, 0, 0, 0, -(w3*1i)/2, 0, 0, (w2*1i)/2, det3*1i - g2/2, (
65                       w3*1i)/2;...
66                       0, 0, 0, 0, 0, 0, 0, 0, 0, 0, 0, 0, -(w3*1i)/2, 0, 0, (w3*1i)/2, 0;...
67                       1, 0, 0, 0, 0, 1, 0, 0, 0, 0, 0, 0, 0, 1, 0, 0, 0, 0, 0, 0, 1];
68     det1(i)=det3;
69     i=i+1;
70 end
71
72 % Steady state conditions i.e :(d_rho = 0)
73
74
75 B=[0;0;0;0;0;0;0;0;0;0;0;0;0;0;0;0;0;0;0;0;0;0;0;0;1];
76
77 % Linear solution:

```

```

62
63 sols=zeros(16,length(Coeffs));
64 for j=1:length(Coeffs)
65     sols(:,j)=linsolve(Coeffs(:,:,j),B);
66 end
67
68 % Visualization:
69
70 figure('Position',[70,70,1300,900])
71
72 subplot(2,1,1)
73 pl = plot(prob_det/(2*pi),imag(sols(2,:)));
74 set(pl,'LineWidth',3.7);
75 set(pl,'LineStyle','-');
76 ylim auto
77 ax=gca;
78 ax.FontSize=30;
79 ax.Box='on';
80 title('', 'FontWeight','bold');
81 xlabel('', 'interpreter','latex');
82 ylabel('Im(\rho_{12})', 'interpreter','latex');
83
84 subplot(2,1,2)
85 pl1 = plot(prob_det/(2*pi),real(sols(2,:)));
86 set(pl1,'LineWidth',3.7);
87 set(pl1,'LineStyle','-');
88 set(pl1,'Color','red');
89 ylim auto
90 ax=gca;
91 ax.FontSize=30;
92 ax.Box='on';
93 title('', 'FontWeight','bold');
94 xlabel('\displaystyle \frac{\Delta_1}{2\pi} \text{ (MHz)}', 'interpreter','latex');
95 ylabel('Re(\rho_{12})', 'interpreter','latex');
96 tightfig;

```

A.2. Self-Consistent Mean-Field Algorithm

MATLAB script containing self-consistent mean-field method is presented. Figures in Section 3.1.2 are obtained by using this script.

```

1 % Self-Consistent Mean-Field algorithm.
2
3 tic % For tracking time it takes to finish the program.
4
5 % for loop that runs over principal quantum number.

```

```

6
7 for n = [0,50,60,70,80,90,100]
8
9     % Constants required to calculate C6 term in atomic units:
10
11     %for Cesium:
12     c0 = 1.064*1e1;
13     c1 = -6.249*1e-1;
14     c2 = 2.330*1e-3;
15
16     C6 = (n^11)*(c0 + n*c1 + (n^2)*c2);
17
18     hartree=4.35574417*1e-18;
19     a0=5.251772108*1e-11;
20     hbar=1.054571800*1e-34;
21
22     % C6 in units of MHz(micrometer)^6
23
24     C6=(1e-6)*C6*hartree*((a0*1e6)^6)/hbar;
25
26     % Number of atoms:
27
28     n_atoms =50;
29
30     % Density of atoms:
31
32     density = 1e9; % cubic centimeters
33
34     % System Parameters (All in units of MHz)
35
36     % Light Field Rabi Frequencies
37
38     w1=2*pi*(0.1);
39     w2=2*pi*(8);
40     w3=2*pi*(1);
41
42     % Field Detunings
43
44     det1=2*pi*(0); % Initially probe detuning is zero.
45     d2=2*pi*(0);
46     d3=2*pi*(-4);
47
48     % Decay Rates
49
50     g1=2*pi*(5.39);
51     g2=2*pi*(3.31);
52
53     % Initial guess for Rydberg State Population:
54

```

```

55     guess=1e-6;
56
57     % Assigning the guess for every atom:
58     pops_ryd=zeros(1,n_atoms);
59
60     for i=1:n_atoms
61         pops_ryd(i)=guess;
62
63     end
64
65     pops_ryd = sum(pops_ryd)/n_atoms;
66
67     % Probe Detuning range to be scanned. Needed for creating coefficient matrix.
68
69     prob_detuning=2*pi*[-8:0.05:3.6,3.6:0.001:4.2,4.2:0.05:8];
70
71     % Number of realizations for statistical averaging.
72
73     n_iteration = 1000;
74
75     for o = 1:n_iteration
76
77         % Initiate atoms at ground state with random positions.
78
79         [atom]=atom_prop(n_atoms,density,d3);
80
81         Coefs_k=[];
82
83         h=1; % Dummy variable
84         m=1;
85
86         for det1=2*pi*[-8:0.05:3.6,3.6:0.001:4.2,4.2:0.05:8]
87
88             %Completing the matrix equation for steady state solutions.
89
90             vec=[];
91
92             for i=17:17:n_atoms*17
93
94                 vec(i,1)=1;
95
96             end
97
98             d4=zeros(n_atoms,n_atoms);
99
100             % Calculates the distance between each atom and assigns the interaction
101             % term with respect to that.
102
103             for i=1:n_atoms

```

```

104
105         for j=1:n_atoms
106
107             if j~=i
108
109
110                 % Calculating the distance between each atom. 10^4 is the
111                 % conversion factor to micrometers.
112                 r = 1e4*sqrt((atom(i,1)-atom(j,1))^2+...
113                     (atom(i,2)-atom(j,2))^2+...
114                     (atom(i,3)-atom(j,3))^2);
115                 d4(i,j) = (C6/r^6)*pops_ryd;
116
117
118             end
119         end
120     end
121
122     % Collects all respective interactions and sums them for each atom.
123
124     for i=1:n_atoms
125
126         d44(i)=sum(d4(i,:));
127
128     end
129
130     % Creating the interaction matrix, later to be added to Coefficient
131     % Matrix.
132
133     int_matrix=[];
134
135     % Terms for the first atom are added manually for simplicity of the
136     % following for loops:
137
138     int_matrix(4,4)=1i*d44(1);
139     int_matrix(8,8)=1i*d44(1);
140     int_matrix(12,12)=1i*d44(1);
141
142     v=1; % Dummy variable
143
144     for k=20:16:16*n_atoms
145
146         for b=k:4:k+8
147
148             int_matrix(b+v,b)=1i*d44(v+1);
149
150         end
151
152         v=v+1;

```



```

152     end
153
154     % Terms for the first atom are added manually for simplicity of the
155     % following for loops:
156
157     int_matrix(13,13)=-1i*d44(1);
158     int_matrix(14,14)=-1i*d44(1);
159     int_matrix(15,15)=-1i*d44(1);
160
161     z=1; % Dummy variable
162
163     for k=20:16:16*n_atoms
164         for b=k+9:k+11
165             int_matrix(b+z,b)=-1i*d44(z+1);
166         end
167         z=z+1;
168     end
169
170     int_matrix(n_atoms*17,n_atoms*16)=0;
171
172     Coefs=[];
173
174     CC=[ 0, (w1*1i)/2, 0, 0, -(w1*1i)/2, g1, 0, 0, 0, 0, 0, 0, 0, 0, 0,
175         0;...
176         (w1*1i)/2, -g1/2 - det1*1i, (w2*1i)/2, 0, 0, -(w1*1i)/2, 0, 0, 0,
177         0, 0, 0, 0, 0, 0, 0;...
178         0, (w2*1i)/2, -d2*1i - g2/2 - det1*1i, (w3*1i)/2, 0, 0, -(w1*1i)/2,
179         0, 0, 0, 0, 0, 0, 0, 0;...
180         0, 0, (w3*1i)/2, -d2*1i - d3*1i - det1*1i, 0, 0, 0, -(w1*1i)/2, 0,
181         0, 0, 0, 0, 0, 0;...
182         -(w1*1i)/2, 0, 0, 0, -g1/2 + det1*1i, (w1*1i)/2, 0, 0, -(w2*1i)/2,
183         0, 0, 0, 0, 0, 0;...
184         0, -(w1*1i)/2, 0, 0, (w1*1i)/2, -g1, (w2*1i)/2, 0, 0, -(w2*1i)/2, g2
185         , 0, 0, 0, 0, 0;...
186         0, 0, -(w1*1i)/2, 0, 0, (w2*1i)/2, -d2*1i - g1/2 - g2/2, (w3*1i)/2,
187         0, 0, -(w2*1i)/2, 0, 0, 0, 0, 0;...
188         0, 0, 0, -(w1*1i)/2, 0, 0, (w3*1i)/2, -d2*1i - d3*1i - g1/2, 0, 0,
189         0, -(w2*1i)/2, 0, 0, 0, 0;...
190         0, 0, 0, 0, -(w2*1i)/2, 0, 0, 0, d2*1i - g2/2 + det1*1i, (w1*1i)/2,
191         0, 0, -(w3*1i)/2, 0, 0, 0;...
192         0, 0, 0, 0, 0, -(w2*1i)/2, 0, 0, (w1*1i)/2, d2*1i - g1/2 - g2/2, (w2
193         *1i)/2, 0, 0, -(w3*1i)/2, 0, 0;...
194         0, 0, 0, 0, 0, 0, -(w2*1i)/2, 0, 0, (w2*1i)/2, -g2, (w3*1i)/2, 0, 0,
195         -(w3*1i)/2, 0;...
196         0, 0, 0, 0, 0, 0, 0, -(w2*1i)/2, 0, 0, (w3*1i)/2, -d3*1i - g2/2, 0,
197         0, 0, -(w3*1i)/2;...
198         0, 0, 0, 0, 0, 0, 0, 0, -(w3*1i)/2, 0, 0, 0, d2*1i + d3*1i + det1*1i
199         , (w1*1i)/2, 0, 0;...

```

```

187         0, 0, 0, 0, 0, 0, 0, 0, 0, 0, 0, -(w3*1i)/2, 0, 0, (w1*1i)/2, d2*1i + d3*1
            i - g1/2, (w2*1i)/2, 0;...
188         0, 0, 0, 0, 0, 0, 0, 0, 0, 0, 0, -(w3*1i)/2, 0, 0, (w2*1i)/2, d3*1i -
            g2/2, (w3*1i)/2;...
189         0, 0, 0, 0, 0, 0, 0, 0, 0, 0, 0, 0, -(w3*1i)/2, 0, 0, (w3*1i)/2, 0;...
190         1, 0, 0, 0, 0, 0, 1, 0, 0, 0, 0, 1, 0, 0, 0, 0, 1];
191
192     % blkdiag is a function that adds the CC Matrix to an Empty Matrix
193     % Coefs diagonally. This for loops allows it to do that for each atom
194     % in the system. For each atom there is a 17x16 matrix involving
195     % coefficients.
196
197     for j=1:n_atoms
198         Coefs = blkdiag(Coefs,CC);
199     end
200
201     Coefs_k(:, :, h) = Coefs + int_matrix;
202
203     % Linearly solving the system using Coefs_k and vec.
204
205     sols=linsolve(Coefs_k(:, :, h), vec);
206     sols_ryd=zeros(1, n_atoms);
207
208     for i=1:n_atoms
209         sols_ryd(i)=real(sols(16*i));
210     end
211     sols_ryd = sum(sols_ryd)/n_atoms;
212
213     s=1;
214     while abs(pops_ryd-sols_ryd)>1e-3
215         s=s+1;
216
217         if s>500
218             %err_d1(m)=d1/(2*pi);
219             m=m+1;
220             break
221         end
222     end
223
224     pops_ryd=sols_ryd;
225     for i=1:n_atoms
226
227         for j=1:n_atoms
228
229             if j~=i
230                 % Calculating the distance between each atom. 10^4 is
                    the
231                 % conversion factor to micrometers.
232                 r = 1e4*sqrt((atom(i,1)-atom(j,1))^2+...

```

```

233             (atom(i,2)-atom(j,2))^2+...
234             (atom(i,3)-atom(j,3))^2);
235         d4(i,j) = (C6/r^6)*pops_ryd;
236
237             end
238         end
239     end
240
241     % Collects all respective interactions and sums them for each atom.
242
243     for i=1:n_atoms
244
245         d44(i)=sum(d4(i,:));
246
247     end
248     % Creating the interaction matrix, later to be added to Coefficient
249     Matrix.
250
251     int_matrix=[];
252
253     % Terms for the first atom are added manually for simplicity of the
254     % following for loops:
255
256     int_matrix(4,4)=+1i*d44(1);
257     int_matrix(8,8)=+1i*d44(1);
258     int_matrix(12,12)=+1i*d44(1);
259
260     v=1; % Dummy variable
261
262     for k=20:16:16*n_atoms
263
264         for b=k:4:k+8
265
266             int_matrix(b+v,b)=1i*d44(v+1);
267
268         end
269
270         v=v+1;
271     end
272
273     % Terms for the first atom are added manually for simplicity of the
274     % following for loops:
275
276     int_matrix(13,13)=-1i*d44(1);
277     int_matrix(14,14)=-1i*d44(1);
278     int_matrix(15,15)=-1i*d44(1);
279
280     z=1; % Dummy variable

```

```

281         for k=20:16:16*n_atoms
282             for b=k+9:k+11
283                 int_matrix(b+z,b)=-li*d44(z+1);
284             end
285             z=z+1;
286         end
287
288         int_matrix(n_atoms*17,n_atoms*16)=0;
289         Coefs_k(:, :, h) = Coefs + int_matrix;
290
291
292         % Linearly solving the system using Coefs_k and vec.
293
294         sols=linsolve(Coefs_k(:, :, h),vec);
295
296         for i=1:n_atoms
297
298             sols_ryd(i)=real(sols(16*i));
299
300         end
301         sols_ryd = sum(sols_ryd)/n_atoms;
302     end
303     solutions(:,h,o)=sols;
304     h=h+1;
305 end
306
307 end
308
309 % Statistical average:
310
311 av_sols= sum(solutions,3)/n_iteration;
312 time=toc;
313 % Save the data.
314 save(strcat('sc_cs_',num2str(n),'_',num2str(n_atoms),'_',num2str(n_iteration),'
           mat'),'av_sols','d11','time','m')
315
316 end

```

A.3. Monte-Carlo Algorithm

MATLAB script containing Monte-Carlo algorithm mentioned in Chapter 4 for rate equation model is provided as follows:

```

1 % This code represents the Monte-Carlo algorithm.
2 % Main loop that runs over each atom.
3 for i=1:n_atoms

```

```

4
5 % Local detuning:
6
7 dloc = atom(i,5);
8
9 % If the atom is in ground state:
10
11 if atom(i,4) == 1
12
13 % Probability of atom leaving ground state:
14
15 p1 = dt*tr11(d1,d2,dloc,w1,w2,w3,g1,g2);
16
17 % Roll a die:
18
19 die = rand;
20
21
22 % Atom leaves ground state if p1 is larger than die:
23
24 if die < p1
25
26 % Probabilities of transitions to states 2,3,4:
27
28 p21 = tr21(d1,d2,dloc,w1,w2,w3,g1,g2)/tr11(d1,d2,dloc,w1,w2,w3,g1,g2);
29 p31 = tr31(d1,d2,dloc,w1,w2,w3,g1,g2)/tr11(d1,d2,dloc,w1,w2,w3,g1,g2);
30 p41 = tr41(d1,d2,dloc,w1,w2,w3,g1,g2)/tr11(d1,d2,dloc,w1,w2,w3,g1,g2);
31
32 die = rand;
33
34 % Check the transitions:
35
36 if die <= p21
37
38 atom(i,4) = 2; % Atom is in state 2
39
40 elseif die <= p21+p31 && die > p21
41
42 atom(i,4)=3; % Atom is in state 3
43
44 else
45
46 atom(i,4)=4; % Atom is in state 4
47
48 % When any atom gets to state 4 or Rydberg state ,
49 % pairwise interactions with every other atom are
50 % calculated and recorded:
51
52 for j=1:n_atoms

```

```

53
54         if j~=i
55             % Inter-atomic distance:
56             r = sqrt((atom(i,1)-atom(j,1))^2+...
57                 (atom(i,2)-atom(j,2))^2+...
58                 (atom(i,3)-atom(j,3))^2);
59             % van der Waals interaction:
60             atom(j,5) = atom(j,5) + C6/r^6;
61         end
62     end
63 end
64 end
65
66 % Same procedure as above for atom being in ground state:
67 elseif atom(i,4) == 2
68
69     p2 = dt*tr22(d1,d2,dloc,w1,w2,w3,g1,g2);
70     die = rand;
71
72     if die < p2
73
74         p32 = tr32(d1,d2,dloc,w1,w2,w3,g1,g2)/tr22(d1,d2,dloc,w1,w2,w3,g1,g2);
75         p42 = tr42(d1,d2,dloc,w1,w2,w3,g1,g2)/tr22(d1,d2,dloc,w1,w2,w3,g1,g2);
76         p12 = tr12(d1,d2,dloc,w1,w2,w3,g1,g2)/tr22(d1,d2,dloc,w1,w2,w3,g1,g2);
77
78         die = rand;
79
80         if die <= p32
81
82             atom(i,4) = 3;
83
84             elseif die <= p42+p32 && die > p32
85
86                 atom(i,4) = 4;
87
88                 for j=1:n_atoms
89
90                     if j~=i
91
92                         r = sqrt((atom(i,1)-atom(j,1))^2+...
93                             (atom(i,2)-atom(j,2))^2+...
94                             (atom(i,3)-atom(j,3))^2);
95
96                         atom(j,5) = atom(j,5) + C6/r^6;
97                     end
98                 end
99
100             else
101

```

```

102         atom(i,4) = 1;
103
104     end
105 end
106
107
108 elseif atom(i,4) == 3
109
110     p3 = dt*tr33(d1,d2,dloc,w1,w2,w3,g1,g2);
111     die = rand;
112
113     if die < p3
114
115         p43 = tr43(d1,d2,dloc,w1,w2,w3,g1,g2)/tr33(d1,d2,dloc,w1,w2,w3,g1,g2);
116         p23 = tr23(d1,d2,dloc,w1,w2,w3,g1,g2)/tr33(d1,d2,dloc,w1,w2,w3,g1,g2);
117         p13 = tr13(d1,d2,dloc,w1,w2,w3,g1,g2)/tr33(d1,d2,dloc,w1,w2,w3,g1,g2);
118
119         die = rand;
120
121         if die <= p43
122
123             atom(i,4) = 4;
124
125             for j=1:n_atoms
126
127                 if j~=i
128
129                     r = sqrt((atom(i,1)-atom(j,1))^2+...
130                             (atom(i,2)-atom(j,2))^2+...
131                             (atom(i,3)-atom(j,3))^2);
132
133                     atom(j,5) = atom(j,5) + C6/r^6;
134                 end
135             end
136
137         elseif die <= p23+p43 && die > p43
138
139             atom(i,4) = 2;
140
141         else
142
143             atom(i,4) = 1;
144
145         end
146     end
147
148 else
149
150

```

```

151     p4 = dt*tr44(d1,d2,dloc,w1,w2,w3,g1,g2);
152     die = rand;
153
154     if die < p4
155
156         p34 = tr34(d1,d2,dloc,w1,w2,w3,g1,g2)/tr44(d1,d2,dloc,w1,w2,w3,g1,g2);
157         p24 = tr24(d1,d2,dloc,w1,w2,w3,g1,g2)/tr44(d1,d2,dloc,w1,w2,w3,g1,g2);
158         p14 = tr14(d1,d2,dloc,w1,w2,w3,g1,g2)/tr44(d1,d2,dloc,w1,w2,w3,g1,g2);
159
160         die = rand;
161
162         if die <= p34
163
164             atom(i,4) = 3;
165
166             for j=1:n_atoms
167
168                 if j~=i
169
170                     r = sqrt((atom(i,1)-atom(j,1))^2+...
171                             (atom(i,2)-atom(j,2))^2+...
172                             (atom(i,3)-atom(j,3))^2);
173
174                     atom(j,5) = atom(j,5) - C6/r^6;
175                 end
176             end
177
178         elseif die <= p24+p34 && die > p34
179
180             atom(i,4) = 2;
181
182             for j=1:n_atoms
183
184                 if j~=i
185
186                     r = sqrt((atom(i,1)-atom(j,1))^2+...
187                             (atom(i,2)-atom(j,2))^2+...
188                             (atom(i,3)-atom(j,3))^2);
189
190                     atom(j,5) = atom(j,5) - C6/r^6;
191                 end
192             end
193
194         else
195
196             atom(i,4) = 1;
197
198
199             for j=1:n_atoms

```



```
200
201         if j~=i
202
203             r = sqrt((atom(i,1)-atom(j,1))^2+...
204                   (atom(i,2)-atom(j,2))^2+...
205                   (atom(i,3)-atom(j,3))^2);
206
207             atom(j,5) = atom(j,5) - C6/r^6;
208         end
209     end
210 end
211 end
212 end
213
214 end
```